Final Report

RESEARCH RELATED TO MEASUREMENTS OF ATOMIC SPECIES IN THE EARTH'S UPPER ATMOSPHERE

Prepared for:

NATIONAL AERONAUTICS AND SPACE ADMINISTRATION
OFFICE OF GRANTS AND RESEARCH CONTRACTS
CODE SC
WASHINGTON, D.C. 20546

CONTRACT NASr-49(30)

STANFORD RESEARCH INSTITUTE
Menlo Park, California 94025 • U.S.A.

STANFORD RESEARCH INSTITUTE
Menlo Park, California 94025 · U.S.A.

Final Report *June 1970*

RESEARCH RELATED TO MEASUREMENTS OF ATOMIC SPECIES IN THE EARTH'S UPPER ATMOSPHERE

By: BERNARD J. WOOD, BILL R. BAKER, and HENRY WISE

Prepared for:

NATIONAL AERONAUTICS AND SPACE ADMINISTRATION
OFFICE OF GRANTS AND RESEARCH CONTRACTS
CODE SC
WASHINGTON, D.C. 20546

CONTRACT NASr-49(30)

SRI Project PGU-6682

Approved:

MARION E. HILL, *Director*
Physical Sciences (Chemistry)

C. J. COOK, *Executive Director*
Physical Sciences Division

C O N T E N T S

CONTENTS (Concluded)

SUMMARY

Accurate interpretation of mass spectral data obtained from a satellite-borne mass spectrometer must include corrections for loss of gaseous atomic species by interaction with the surfaces of the analytical instrument itself. Atomic oxygen and atomic hydrogen are the atmospheric constituents of particular concern at altitudes greater than 120 km. We studied the kinetics of interaction of these species (under conditions similar to those encountered in this atmospheric region) on surfaces of engineering interest, viz. gold, silver, titanium, stainless steel, and aluminum. The results of our study provide some insight into the mechanisms of these processes. Our data and analysis supply a basis for interpretation of existing information reported by flight mass spectrometers and for the design of new instruments for atmospheric exploration.

In our experimental measurements of atom loss, we employed an ultrahigh vacuum system incorporating a cylindrical reaction vessel in which the total gas pressure and the entering flux of atoms were held constant. Atoms were generated at the inlet of the reactor by thermal dissociation of oxygen or hydrogen on a hot tungsten ribbon. The flux of atomic species that survived transit through the reactor was determined by a mass spectrometer with its ion source adjacent to the reactor outlet. We evaluated the relative rate of atom loss on a particular surface by observing the diminution in atom flux at the outlet when a specimen of the material of interest was inserted into the reactor. Interpretation of the data to yield atom loss coefficients was facilitated by means of an analytical model of the experiment. This model is based on the assumption that atomic particles incident, but not lost, on the reactor surface obey a cosine scattering law. Upon specification of a loss coefficient α indicative of the probability that an atom will be removed from the gas phase upon collision with the wall, the model predicts the intensity of the atom flux at the outlet as a function of α and of reactor geometry.

We measured atom adsorption, desorption, and recombination rates

on the metal surfaces by means of standard flash-filament techniques. With the same method we evaluated the surface interactions of the common gaseous impurity, carbon monoxide.

Our results suggested that the dominant oxygen atom removal mechanism on gold is gas atom-adatom (Eley-Rideal) recombination. By way of contrast, the atom recombination rate on silver is small relative to the rate of occlusion (or reaction) of the oxygen atoms in the silver metal. Numerical values are given for the rates of oxygen atom interaction with these two metals. Consequently, the kinetic data may be employed to estimate the magnitude of oxygen atom loss in the sampling antechambers of flight mass spectrometers with silver or gold surfaces.

Titanium forms a spectrum of stable solid phase oxides upon exposure to oxygen atoms. The interactions were too complex to deduce useful kinetic parameters. We concluded that the use of this metal in a flight mass spectrometer might lead to unpredictable behavior with respect to oxygen atom loss.

The interaction of oxygen atoms with type 302 stainless steel varied with the pretreatment of the surface, although in general this metal possesses a greater loss efficiency for oxygen atoms than did the noble metals. Under certain conditions, oxygen atoms reacted with carbon in the steel surface to produce carbon dioxide. We felt that any stainless steel employed in a flight mass spectrometer would require direct empirical examination of the kinetics and the products of oxygen atom-surface interaction on a specimen of composition and pretreatment identical to that in the flight instrument.

Our aluminum specimen was oxide-covered and virtually inert to oxygen atom recombination or reaction. Hence, from this standpoint we consider aluminum to be an excellent candidate for the surfaces of components in flight mass spectrometers.

A low sticking efficiency and high gas atom-adatom recombination rate constant for hydrogen atoms on gold limit the adatom surface coverage to less than 0.1 monolayer. On gold saturated with a monolayer of adsorbed oxygen, colliding hydrogen atoms react with nearly unit effi-

ciency. We could not determine the product of this encounter, but if it is a metastable species such as the OH radical, hydrogen atoms could still be effectively transported through an oxygen-covered gold antechamber.

Our results for oxygen atom and hydrogen atom interaction with gold are basically consistent with the data reported by the OGO-F satellite mass spectrometer with a gold-plated antechamber. We conclude that refinement of our analytical model to fit the geometry of the OGO-F antechamber would enable precise corrections for atom loss to be applied to the number density values of atmospheric atomic oxygen obtained with this instrument. Such a study would be a timely subject for further research in this area.

LIST OF ILLUSTRATIONS

ILLUSTRATIONS (Concluded)

TABLES

I. INTRODUCTION

The problem of evaluation of the atomic oxygen concentrations in the earth's upper atmosphere from data reported by rocket- and satellite-borne mass spectrometers has been amply documented by a number of independent investigators.[1] It is generally agreed that the true atom number density in the vehicle's environment is higher than that reported by the on-board mass spectrometer. The high reactivity of oxygen atoms is the apparent cause for such atom loss. These species can interact with solid surfaces by adsorption, by formation of oxides, and by catalytic production of molecular oxygen. Similar considerations apply to other reactive species, including atomic hydrogen, which might be atmospheric constituents. Consequently an understanding of the respective rates and mechanisms of these atom-solid interactions on specific surfaces employed in flight mass spectrometers is essential to an interpretation of data on upper atmosphere composition.

II. OBJECTIVE

The objective of this project was to elucidate the kinetics and mechanisms of interaction of atomic species, principally oxygen, with surfaces of engineering interest under conditions similar to those encountered in the upper atmosphere.

III. APPROACH TO THE PROBLEM

A. Design of the Experiment

1. Atom-Surface Interactions of Interest

Mass spectrometers are useful for investigation of the earth's atmosphere at altitudes greater than 120 km. At this height the total particle number density is equivalent to a pressure of about 10^{-5} torr and the major atmospheric constituents are atomic oxygen and molecular nitrogen. As one goes higher, the total particle number density diminishes but the ratio of oxygen atoms to nitrogen molecules increases. Atomic hydrogen may be a minor atmospheric constituent at altitudes

greater than 200 km.

Flight mass spectrometers used to investigate this region of the atmosphere have been, in large measure, constructed from stainless steel. A number of specific instruments, however, have used other materials for construction, particularly in the ion source region, for the purpose of mitigating the rate of atom loss. These materials include titanium (AFCRL OV-36 satellite), silver (Explorer XXXII satellite), and gold (OGO-F satellite).

As a consequence of this information, we oriented our experimental studies to examine primarily the interactions of oxygen atoms with stainless steel, titanium, silver, gold, and aluminum, the last metal being a common, low-cost material of construction of reportedly[2] low activity for oxygen atom recombination. The interaction of hydrogen atoms with gold and oxygen-covered gold was also investigated.

In general, four elementary processes can be postulated to cover all modes of atom-surface interactions that result in loss of atoms from the gas phase. These include:

a. adsorption (capture) - desorption (reflection)
b. occlusion (reaction with solid phase)
c. recombination
d. reaction with other adatom species.

Our experimental objective was to discern and evaluate quantitatively the role of each of these processes in each of the gas/solid systems studied. We were able to do this for the oxygen-gold, oxygen-silver, and hydrogen-gold systems; the other systems exhibited complexities, such as the formation of multiple, solid-phase oxides, which enabled us to measure only the relative total atom loss coefficient under the experimental conditions.

2. Basis of the Experimental Approach

Our experimental approach employs a reaction vessel in which the total gas pressure and the entering flux of atoms are held constant. We evaluate the rate of interaction of atoms with a metal surface by observing the diminution in atom flux at the outlet of the vessel when a speci-

men of the material of interest is inserted into the reactor.

The experimental apparatus (Fig. 1) consists of a cylindrical reaction vessel through which atoms flow from a source at one end to a high-capacity vacuum pump at the opposite end. Under the conditions of molecular flow, which apply throughout the pressure range 10^{-5} to 10^{-9} torr employed in this apparatus, simple kinetic theory suggests that once an atom enters the reactor it will depart through the exit or the entrance aperture after suffering multiple collisions with the reactor wall. However, if the atom adsorbs, recombines, or reacts with the wall during one of these collisions, it will remain in the reactor or leave it as a molecule. To use such an apparatus to measure quantitatively the total atom loss rate on the reactor surface, it is necessary to have an analytical model that describes the distribution of atom flux within the vessel as a function of its dimensions and the atom "capture" probability of its interior surfaces.

B. Analytical Model of the Experiment

A cylindrical geometry was chosen for reasons of experimental convenience, but also because cylindrical sampling antechambers have been used with a number of flight mass spectrometers, including that on the OGO-F satellite. In our experiments we measured the flux of atoms which survived transit through the reactor with and without metal specimens. Consequently the analytical model was formulated to predict the atom flux at the reactor exit as a function of the atom loss probability on the wall. The geometry of our model is sketched in Fig. 2.

Under the conditions of our experiments the flow through the reactor can be described in terms of the flux of atoms. There is essentially no interaction between gaseous atoms in the interior of the chamber because of the low number density. However, when atoms strike the wall they may be temporarily held and reemitted, they may combine with other atoms to be emitted as molecular oxygen, or they may become strongly bound to the surface as adsorbed or occluded atoms.

Under these conditions the flow can be treated as a radiation problem involving the steady-state flux of atomic oxygen, and the inter-

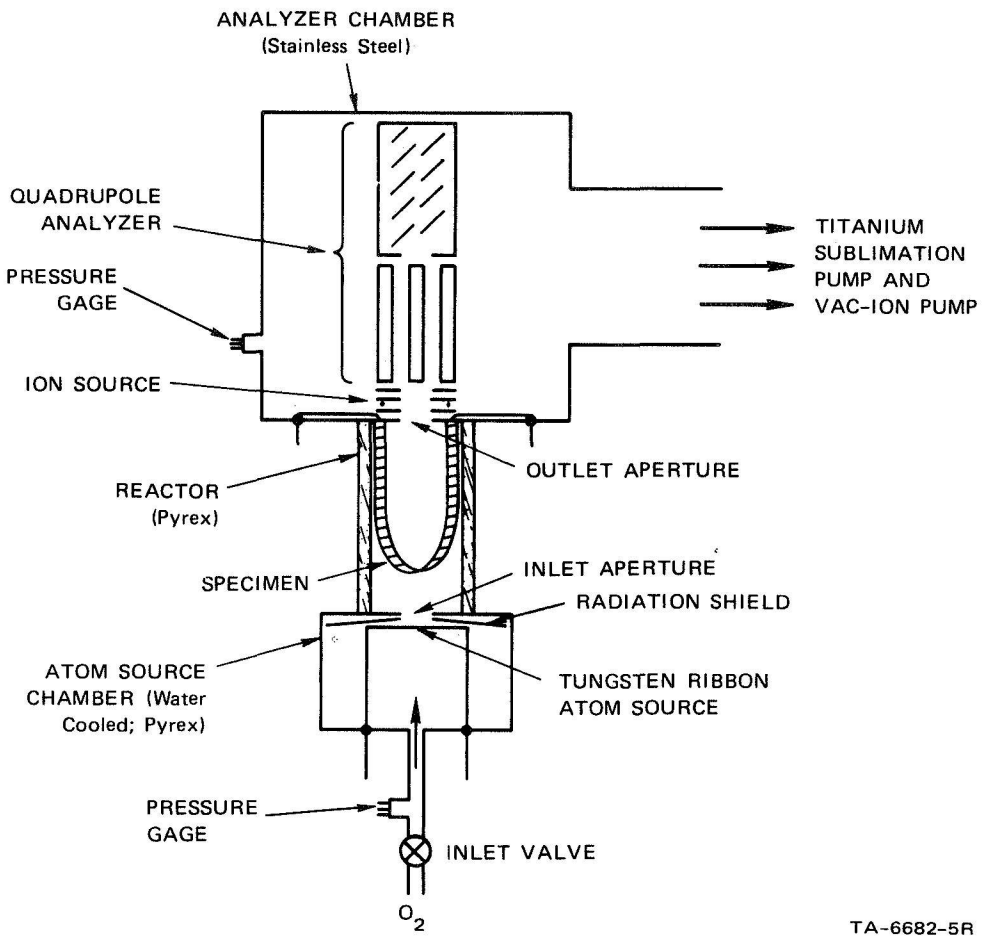

FIGURE 1 SCHEMATIC DIAGRAM OF APPARATUS. Specimen may be lining on wall of reactor (not shown) or, for flash filament experiments, a ribbon suspended inside the reactor (as shown).

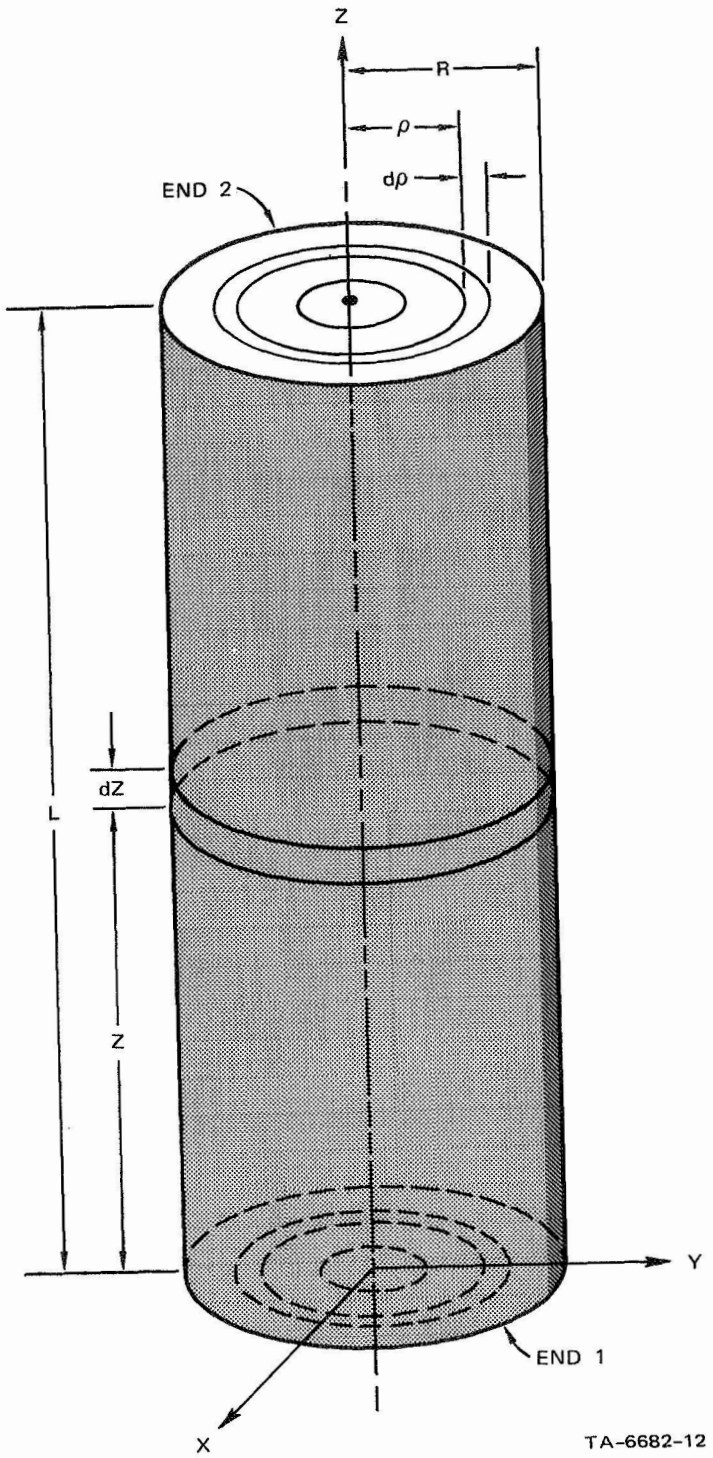

FIGURE 2 REACTOR MODEL

action with the wall is described by a loss coefficient α. This loss coefficient α is defined as the probability that an atom will be removed from the gas phase upon collision with the wall.

It is assumed that the flux density, i.e., number of particles emitted per unit solid angle per unit area of the emitter per unit time, obeys Lambert's law, that is, varies as the cosine of the angle between the normal to the emitting surface and the direction of the flux. The variation of flux intensity emitted from dA is indicated by the circle in Fig. 3a.

The solid angle subtended by an area element dB at A is

$$d\Omega = \frac{dB \cos \theta_b}{\ell^2} \tag{1}$$

If the flux emitted per unit area from dA is of intensity E_o in the direction of the normal n_a, then the total flux transmitted from dA to dB is

$$dE_{dA \to dB} = E_o \, dA \, dB \, \frac{|\cos \theta_a \cos \theta_b|}{\ell^2} \tag{2}$$

It is convenient to introduce an influence function or angle factor w_{AB} defined by

$$w_{AB} \equiv \frac{dE_{dA \to dB}}{E_o \, dA dB} = \frac{|\cos \theta_a \cos \theta_b|}{\ell^2} \tag{3}$$

From the definition it follows that w is symmetric or $w_{AB} = w_{BA}$.

In order to simplify the discussion we will consider for the present a general convex body of rotation such as the egg-shaped vessel shown in Fig. 3b. The surface is convex so that each element of area can be seen by every other element.

An axially symmetric distribution of flux is considered. We formulate the influence function for two conical ring elements with surfaces inclined at angle β from the axis as sketched in Fig. 3c. By straightforward vector algebra described in Appendix A, we can obtain the influence function for the two rings

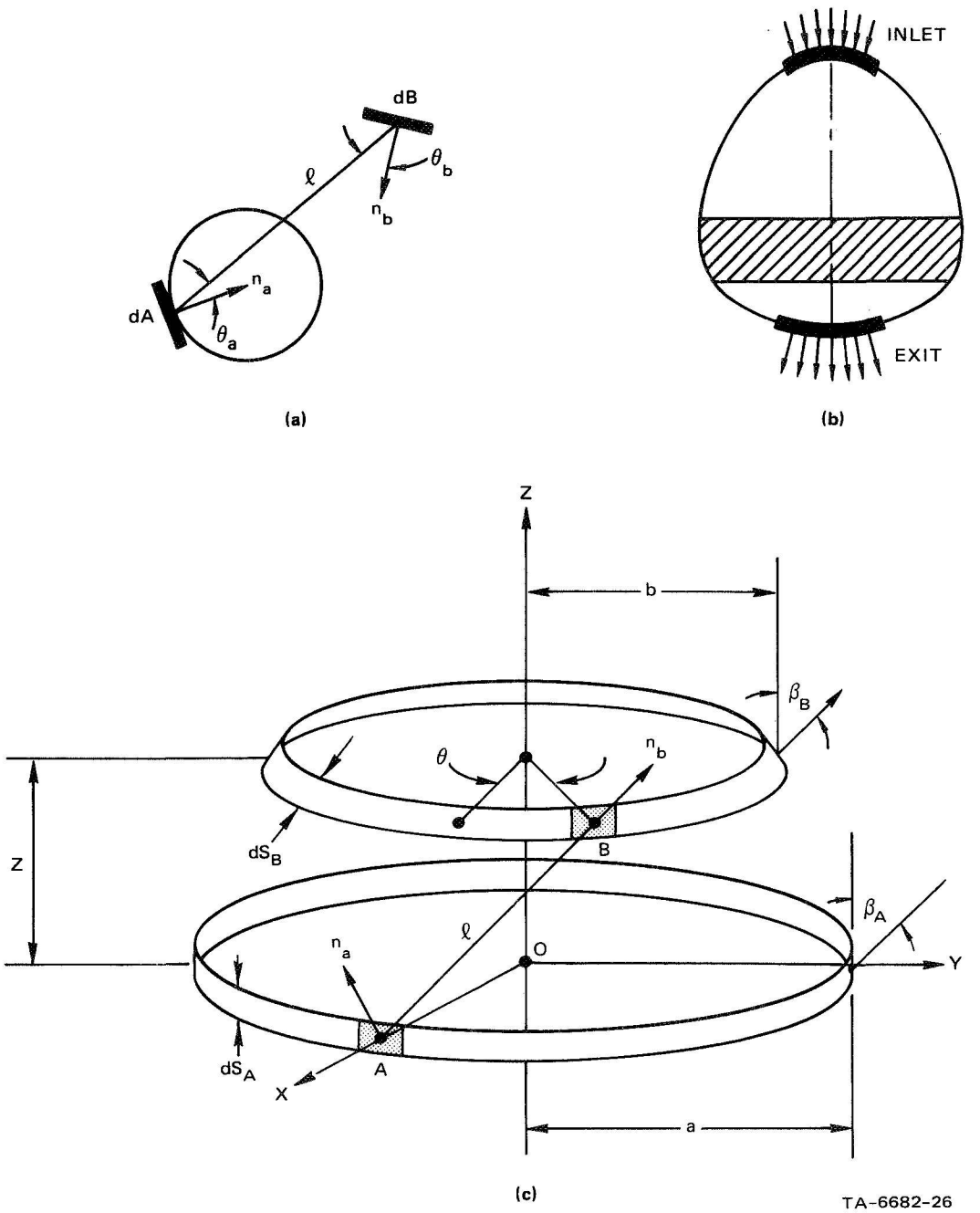

FIGURE 3 CONVEX BODY OF ROTATION

$$w_{AB} = w_{BA} = \frac{dE_{r_B \to dA}}{E_B \, dAp \, (2\pi b \, dS_B)} = \frac{1}{2\pi} \int_0^{2\pi} \frac{|\cos \theta_A \cos \theta_B|}{\ell^2} \, d\theta =$$

$$\left| \sin \beta_A \sin \beta_B \left\{ - \frac{1}{4ab} \left[1 + (a^2-b^2-z^2)G \right] + (b^2-z^2-a^2) \frac{a}{2b} \frac{\partial G}{\partial (a^2)} \right\} \right. \qquad (4)$$

$$\left. + \cos \beta_B \sin \beta_A \, za \frac{\partial G}{\partial (a^2)} - \cos \beta_A \sin \beta_B \, zb \frac{\partial G}{\partial (b^2)} - \cos \beta_A \cos \beta_B \, z^2 \frac{\partial G}{\partial (z^2)} \right|$$

where the basic elementary integral is

$$G = \frac{1}{2\pi} \int_0^{2\pi} \frac{d\theta}{z^2+a^2+b^2-2ab \cos \theta} = \frac{1}{\left[(z^2+a^2+b^2)^2 - 4a^2b^2 \right]^{1/2}} \qquad (5)$$

Equation (4) can also be specialized as is shown in Appendix A if the angles β_A and β_B are set to either zero or $\pi/2$ to get the standard relations for elements of our right circular cylindrical reactor.

Now we can formulate the balance of flux. For the axially symmetric problems considered here we can use any parameter, say x, which locates a conical ring element along the meridian. The parameter may later be set equal to arc length along the meridian or it may be any other convenient variable.

Let the incident flux or number of particles striking a unit area per unit time be denoted by

$$f(x) = \text{incident flux at location x along meridian} \qquad (6)$$

and let the fraction of particles lost be

$$\alpha(x) = \text{loss coefficient at location x} \, . \qquad (7)$$

Then the <u>total</u> flux density per unit area per unit time emitted at x is

$$\text{total flux out} = f(x) \left[1-\alpha(x) \right] \qquad (8)$$

However, if the flux density is E_o normal to the emitting surface and Lambert's law holds, then integration over all directions shows that the total flux leaving the surface is $E_o \pi$. Combining this result with Eq. (8) gives

$$E_o(x) = f(x) \frac{\left[1-\alpha(x) \right]}{\pi} \qquad (9)$$

The total incident flux density at any station x has its source in the flux emitted from all the other stations t of the body. From the basic definition of the influence (angle) function (3) we have

$$f(x) = \frac{dE(x)}{dA(x)} = \int w\ (x,t)\ E_o(t)\ da(t)$$

or

$$f(x) = \int_L w\ (x,t)\ f(t)\ [1-\alpha(t)]\ \frac{2\pi r(t)}{\pi}\ ds(t)$$

$$= 2 \int_L w(x,t)\ f(t)\ [1-\alpha(t)]\ r(t)\ ds(t) \qquad (10)$$

The last equation represents the flux balance for a concave body radiating under steady-state conditions. The equation is homogeneous, and we know from physical arguments that there are no eigenfunctions or homogeneous solutions if the absorption coefficient α is not identically zero. In that case at least a portion of the surface adsorbs part of the particles that strike it. Since every portion does emit onto the absorbing surface, particles would be lost continuously and a steady-state solution could not exist.

Eq. (10) can be modified to account for axially symmetric inlet and exit areas. For example, an exit such as the one leading to the mass spectrometer allows no particles to return to the chamber, so the area of the exit appears to have complete absorption (α=1). The integral taken over that portion of the surface gives no contribution.

An inlet with specified flux density E_o emitted normal to a surface element of the entrance can be represented if we extract that portion of the integral (10) taken over the inlet and prescribe the values of f and α according to (9). If we use L_c to denote the total portion of the meridian left after extracting all exits and inlets, then (10) can be written

$$f(x) = 2 \int_{L_c} w\ (x,t)\ f(t)\ [1-\alpha(t)]\ r(t)\ ds(t) + 2\pi \int_{L_{inlet}} w\ (x,t) E_o(t) r(t) ds(t) \qquad (11)$$

The question of the uniqueness of solution of this Eq. (11) can be treated in a manner similar to that of the closed container. The

homogeneous problem--obtained by setting $E_o(x) \equiv 0$ in (11)--corresponds to a complete vessel with perfect absorption (α=1) over all inlet and exit surfaces. As we saw before, such a problem has no steady-state solution so (11) has no homogeneous solutions. Since the kernel function

$$C(x,t) = 2w(x,t)\,[1-\alpha(t)]\,r(t)\,\frac{ds}{dt} \tag{12}$$

is bounded, it follows from the Fredholm alternative[3] that the inhomogeneous system (11) always has a unique solution for any distribution $E_o(x)$ of flux over the inlet area.

The solution of Eq. (11) by analytic methods seems to be impossible because of the relatively complicated kernel functions $w(x,t)$. Therefore, numerical methods have been developed. The essential step is the replacement of the integral (11) by a finite sum involving the values of f at discrete points of the meridian.

The first approach used a simple Riemann sum to approximate the integral. The meridian was divided into a finite number of segments of nearly equal size. The values of the flux and of the kernel at the midpoint were multiplied by the width of the interval to give the approximate contribution to the integral. Thus Eq. (11) was discretized or converted to a corresponding finite system of linear algebraic equations for the values of the flux at the midpoints of the intervals. That system of algebraic equations was solved by a Gaussian elimination procedure.

When the length L of the cylindrical chamber is very large compared to the radius R_o, then very many elements are necessary to obtain a satisfactory representation of the integral by means of a Riemann sum. For such long geometries, better accuracy and shorter computation times were obtained by using Simpson's rule to represent the integral as suggested by Sparrow et al.[4], who also used an iterative technique to solve some thermal radiation problems for cuplike holes. We found that modification of conventional iterative techniques to extrapolate from two previous solutions to predict the next trial solution gave a further reduction in computation time. An indication of the accuracy of the calculation was obtained by a mass balance based upon the flux distribution.

The total flux absorbed per unit area is given by the product of $f\alpha$. This product is then integrated in the same approximate manner over the wall. Since the exit has been formally represented by setting $\alpha \equiv 1$, it follows that the total exit flux is given by a corresponding integral of $f\alpha$ over the exit area. Besides the flux leaving the exit and the particles sticking on the walls, there are some additional particles that bounce back through the entrance from each portion of the container walls. That is, our specification of the emitted flux $E_o(x)$ at the inlet using Eq. (9) takes no account of the actual incident flux or a flux balance. We assume that the actual steady-state output of the atom source is independent of the fraction of atoms leaving the reactor by way of the inlet. These atoms are considered to be irrevocably lost from the reactor.

The object of the calculations is to find the relationship of the total flux leaving the chamber as a function of the absorption coefficient of a cylindrical band which forms a portion of the wall. A series of calculations is made in which the inlet flux is held constant (at a nominal value of 1.0), the geometry is fixed, and the total exit flux is calculated for various values of α_{band}. The exit flux is then normalized with respect to the total output for the case where the band has zero loss; i.e., the band behaves just like a nonabsorbing glass wall which forms the reference for the experimental case.

The flux distributions for several values of α_{band} are shown in Figs. 4 and 5, for different geometries of the reactor vessel and band. Plots of the normalized exit flux as functions of α_{band} and reactor geometry are shown in Fig. 6.

Calculations have been carried out satisfactorily for reactor geometries with length/radius ratio values as large as 6. When the chamber is relatively long with small inlet and outlet, then a large number of intervals must be used in order to provide a good approximation of the integral. In such cases, the time required to solve the system of equations increases rapidly. Although the schemes described in some measure allow this problem to be bypassed, computational difficulties still show up. We are optimistic, however, that a modest additional effort on this

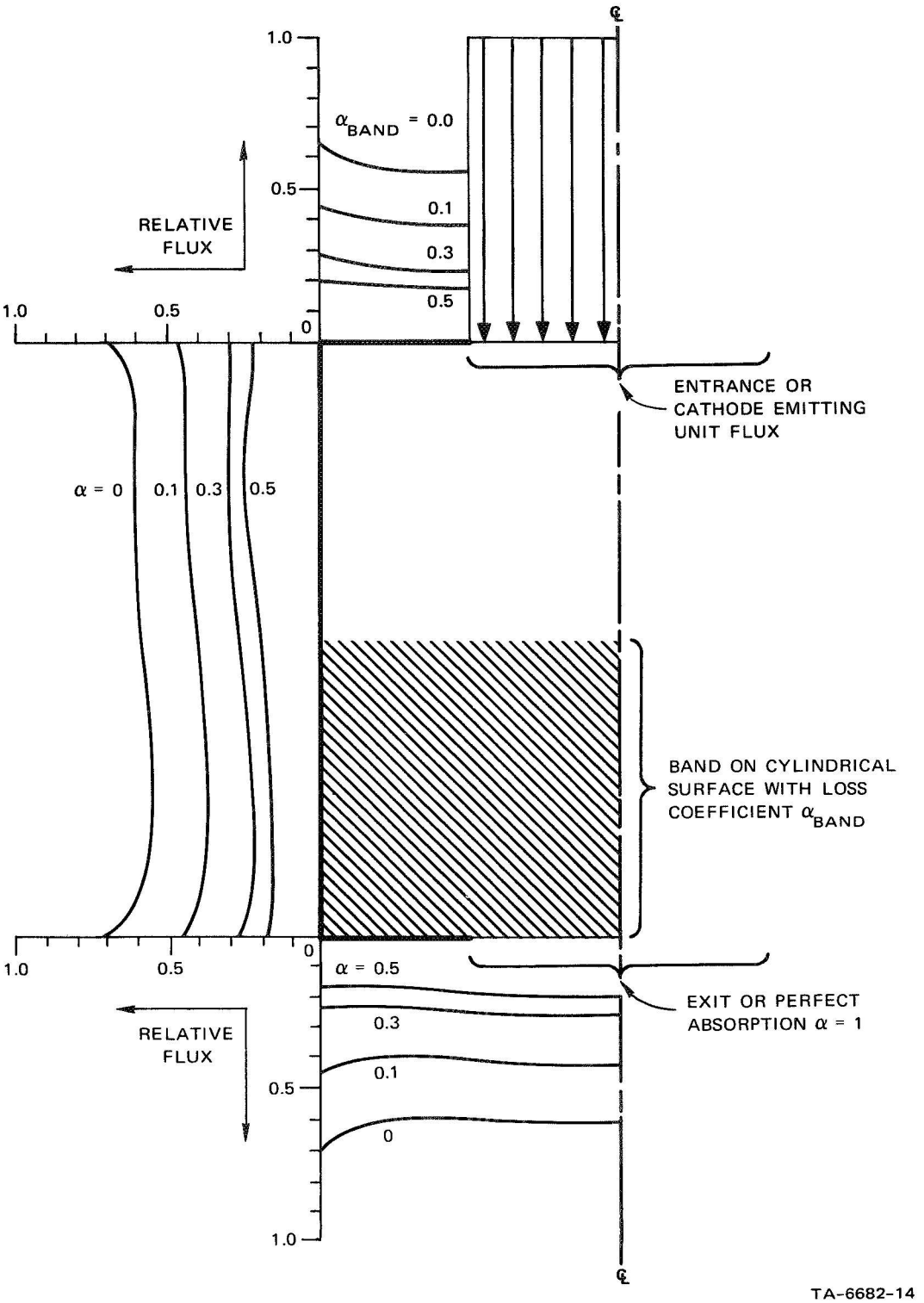

FIGURE 4 DISTRIBUTION OF INCIDENT FLUX ON WALL AND OPENINGS OF REACTOR FOR FOUR VALUES OF α_{band}. Relative dimensions: R_o = 1, L = 2, R_{in} = 0.5, R_{ex} = 0.5, h_{band} = 1.

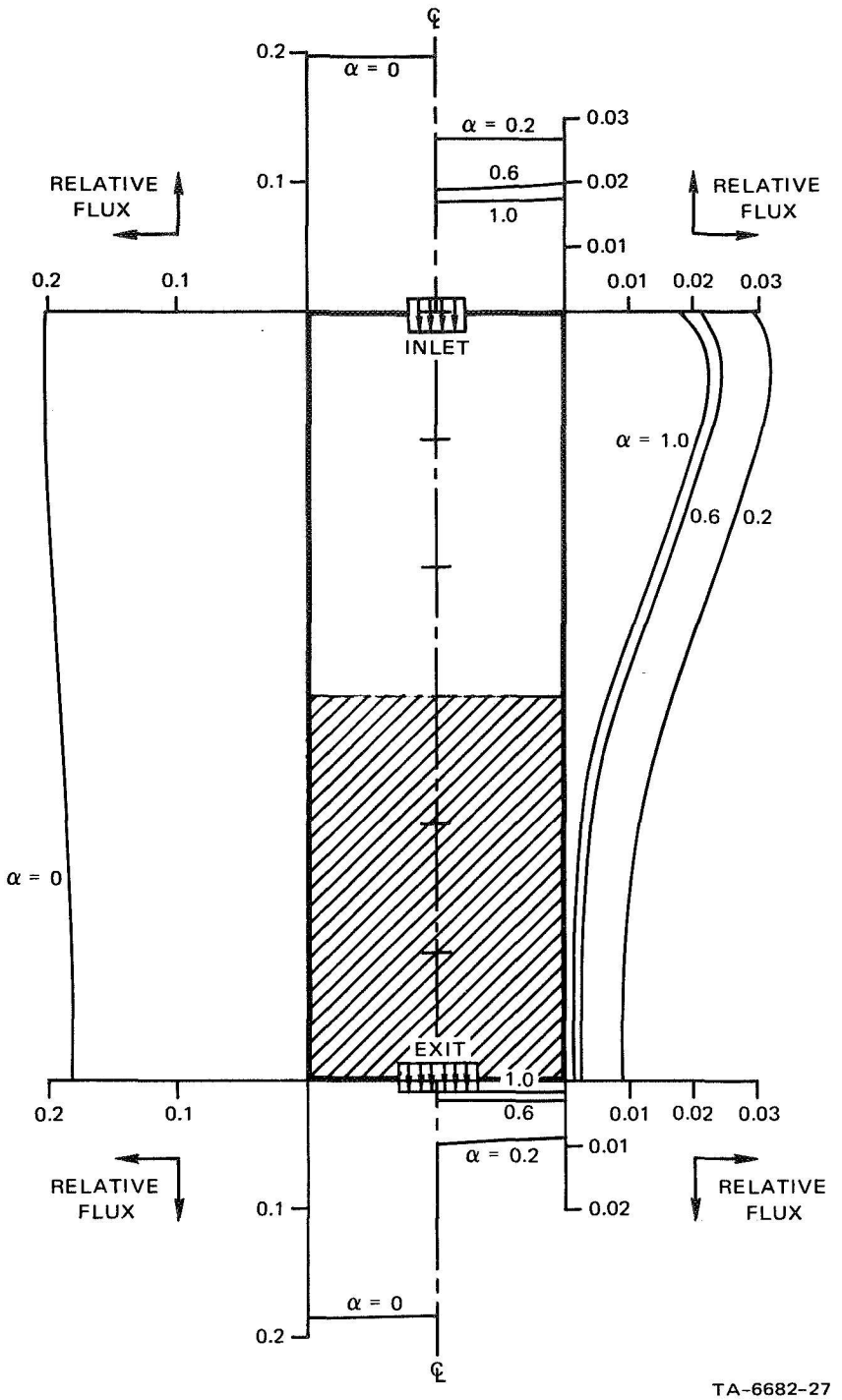

FIGURE 5 DISTRIBUTION OF INCIDENT FLUX ON WALL AND OPENINGS OF REACTOR FOR FOUR VALUES OF α_{band}. Relative dimensions: R_o = 1.0, L = 6.0, R_{in} = 0.118, R_{ex} = 0.245, h_{band} = 3.0. (Note that the more uniform distribution for α_{band} = 0 is shown on the left side of the reactor chamber with a different scale. Unit inlet flux is not indicated in figure.)

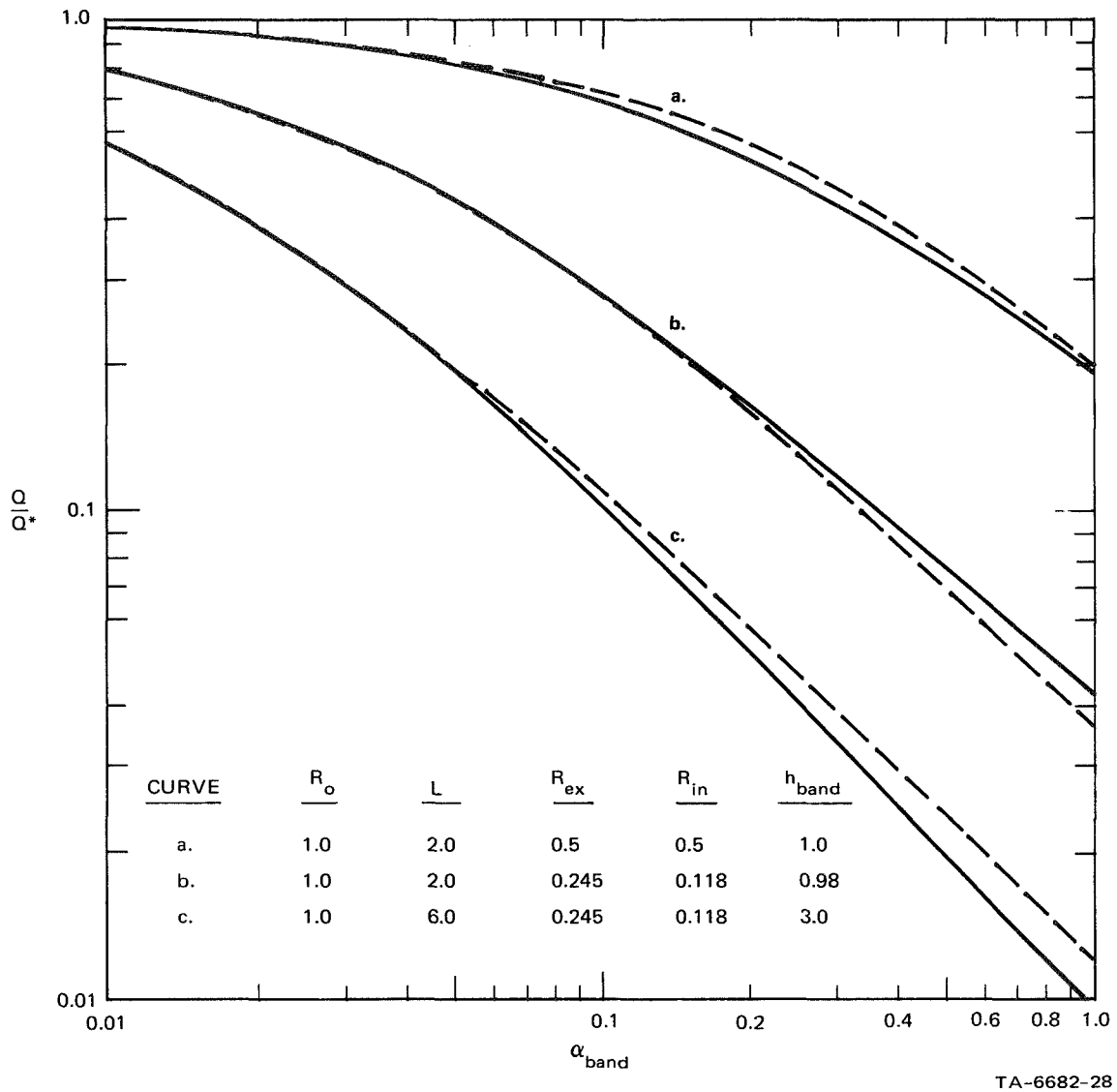

FIGURE 6 RELATIVE OUTLET FLUX AS A FUNCTION OF α_{band} FOR THREE DIFFERENT GEOMETRIES. Solid curves were obtained from the numerical analysis; dashed curves, from the uniform flux assumption, Eq. (14).

problem would lead to successful solutions for length/radius ratio values at least as great as that of the OGO-F antechamber, viz. Eq. (11).

Results of our computation for a reactor with $L/R_o = 2$ (Fig. 4) show that the flux distribution on the walls is nearly constant. This suggests a simple approximate method of calculating the flux density. A simple balance of the incoming particles with those which stick on the absorptive band or leave through the openings gives for the exit flux

$$f_o = \frac{R_{in}^2}{R_{in}^2 + R_{ex}^2 + 2\alpha_b R_o h_b} \tag{13}$$

where h_b is the height of the absorbing band.

The total mass flow rate Q through the exit is obtained by multiplying f_o by the exit area. It is convenient to normalize Q to the case of a reactor with nonabsorbing walls ($\alpha_{band} = 0$) with an exit flow rate of atoms designated Q*

$$\frac{Q}{Q^*} = \frac{R_{in}^2 + R_{ex}^2}{R_{in}^2 + R_{ex}^2 + 2\alpha_b R_o h_b} \tag{14}$$

The results of this simple analysis are shown as dashed lines in Fig. 6 for three different geometries; two short chambers and one long chamber. Equation (14) gives results that compare favorably with the results of the finite element calculations shown as solid curves. The approximate solution is better if the chamber is shorter (i.e., more nearly spherical in shape) and if the absorption coefficient is low. Examination for the longer geometry (Fig. 5) shows larger variations in the flux distribution so that Eqs. (13) and (14) are less accurate. Nevertheless, those simple formulas provide considerable insight into the system and could be used for preliminary design of experiments or instruments.

C. Experimental Apparatus and Procedure

1. Apparatus

Our reactor (Fig. 1) is a cylinder of pyrex or quartz situated in an ion-pumped, ultrahigh vacuum system. Most of our data were ob-

tained with a pyrex reactor of 2.2 cm inside diameter and 12 cm length.

Atoms are generated by thermal dissociation of molecular oxygen on an electrically-heated tungsten ribbon in a water-cooled chamber at the lower end of the reactor. The reactor inlet is a 0.25-cm radius hole in a 0.3-cm thick glass plate situated in close proximity to the tungsten ribbon. A radiation shield of tungsten foil between the hot ribbon and the glass plate prevents overheating of the glass parts of the reactor in this vicinity. Based on the geometric conductance[5] of this inlet, a central area of approximately 0.02 cm^2 on the tungsten ribbon surface had line-of-sight access to the interior of the reactor. Hence, the total steady-state mass flow rate of atoms into the reactor is assumed to be the integrated flux emitted from this region of the tungsten ribbon at a fixed temperature and oxygen pressure. At tungsten temperatures greater than 2100°K, it has been shown[6] that the emitted flux of oxygen atoms is more than an order of magnitude greater than the emitted flux of any volatile tungsten oxide. Consequently, we always conducted our experiments with the central portion of the tungsten ribbon at temperatures in excess of 2100°K as measured by an optical pyrometer. Oxides that formed and evaporated from the cooler end portions of the tungsten ribbon were denied access to the reactor by virtue of the small effective inlet aperture diameter, and thus they were permanently trapped in the source chamber by condensation on the cooled walls.

The reactor outlet is a 0.55-cm radius hole in an 0.3-cm thick glass plate, which leads directly to a large chamber pumped to low pressure by a titanium sublimation pump and an ion getter pump. This chamber contains a quadrupole mass spectrometer* placed so that its ion source is immediately adjacent to the reactor exit. The pressure in the system is measured by ion gages near the oxygen inlet and on the analyzer chamber.

The analytical model considers the case where a portion of the reactor wall is covered by a metal specimen. In a number of experiments, we mounted metal-foil specimens in our reactor in this fashion. Such

---

* Model QUAD 250, Electronic Associates, Inc., Palo Alto, California

specimens, however, could not be readily flash-heated to measure adsorption and desorption rates. Hence, we also employed specimens in the form of ribbons with a length of approximately 20 cm and a width of about 0.5 cm. These ribbons were suspended from their ends on electrical feedthroughs at the upper end of the reactor. We demonstrated, using a wall liner of silver foil identical in source, pretreatment, and geometric surface area to that of a silver ribbon, that the measured atom loss for the two specimen geometries coincided when the wall liner was situated adjacent to the outlet end of the reactor. It was possible, therefore, to employ the convenient ribbon specimen geometry with full confidence that measured atom loss characteristics could be interpreted in terms of our analytical model. Also, for cases where reactor and specimen geometry were unchanged, and the oxygen pressure and source temperature were constant, the relative atom loss characteristics of various metals could be evaluated by a comparison of the fraction of atoms measured in the reactor effluent for each specimen.

2. Mass Spectrometer Calibration

The geometry of the apparatus is such that the mass spectrometer detects the effective flux of species emerging from the exit aperture of the reactor. For calibration, the total mass flow of gas Q through the reactor was computed from measured pressure differences between the inlet and analyzer ion gages and the calculated overall conductance[5] of the apparatus between these two pressure-measuring points. In the range $10^{-6} < Q < 10^{-3}$ torr-liter/sec, the mass spectrometer signal was found to be proportional to Q. The observed values of Q, together with the values of conductance F calculated from the apparatus geometry, enabled us to compute the steady-state pressure P in any part of the system from the basic Knudsen flow equation:

$$Q = F(P_2 - P_1) \tag{15}$$

The mass spectrometer was calibrated before and after each experiment to allow corrections for electron multiplier sensitivity. Also, cracking patterns for the gases of interest were determined empirically, and the mass spectrometer was operated at a fixed resolution setting for

the entire series of experiments.

3. Experimental Procedure

a. Total Atom Loss Measurement. The total loss of atoms due to interactions at the surfaces in the reactor is related to the surviving fraction of atoms measured in the reactor effluent. Of course, even in a reactor with completely inert and noncatalytic walls, the steady-state absolute flux of atoms at the outlet must be less than that at the inlet by the factor representative of the net transmission probability[7] of the reactor and its apertures. We computed the net transmission probability of our apparatus from formulas for molecular flow through cylindrical tubes.[5,7] We used this figure to predict the atom flow rate through the outlet of the empty reactor from the kinetic data of Schissel and Trulson[6] for oxygen dissociation on a hot tungsten surface. A comparison of these flow rates with those actually measured (Table I) indicates that atom loss on glass and quartz is negligibly small. This conclusion was confirmed in an experiment in which the radius of the exit hole was reduced to a degree such that the number of wall collisions by atoms in the reactor approximately doubled. This change caused no variation in the fraction of atoms in the effluent within the precision of our measurement. These observations are in agreement with reported[2] values of the catalytic activity of glass and quartz for oxygen atom recombination ($\gamma \cong 10^{-4}$, i.e., only one out of 10^4 collisions results in atom loss by recombination).

We determined relative atom loss for each metal by making separate measurements of the fractional atom flux Q_O/Q_{O_2} in the reactor effluent, over a range of source temperatures T_w and source oxygen pressures, with and without metal specimens in the reactor. Typical results for wall specimens of silver foil in two different reactors are shown in Fig. 7.

b. Atom Adsorption Rate Measurements. Atoms were adsorbed or occluded by the metal ribbon specimens during their exposure to a fixed and constant atom flux. Following this exposure, we heated the ribbon to a high temperature (well below the melting point) by passing an elec-

Table I

SURVIVAL OF OXYGEN ATOMS IN PYREX AND QUARTZ REACTORS

(Tungsten Ribbon Source Temperature: 2150 ± 25°K)

Reactor Dimensions		P_{O_2} (Calculated)	Atom Mass Flow Rate at Reactor Outlet	
Length (cm)	Diameter (cm)	in Source Chamber (torr) × 10^4	Measured (torr-ℓ/sec)×10^7	Predicted from[a] Data in Ref. 6 (torr-ℓ/sec)×10^7
12	2.2	0.50	3.5	3.4
		2.5	11	9.2
5.1	5.1	0.48	15	9.1
		4.3	83	36

[a] Corrected for total transmission probability of reactor assuming no loss of atoms on reactor wall.

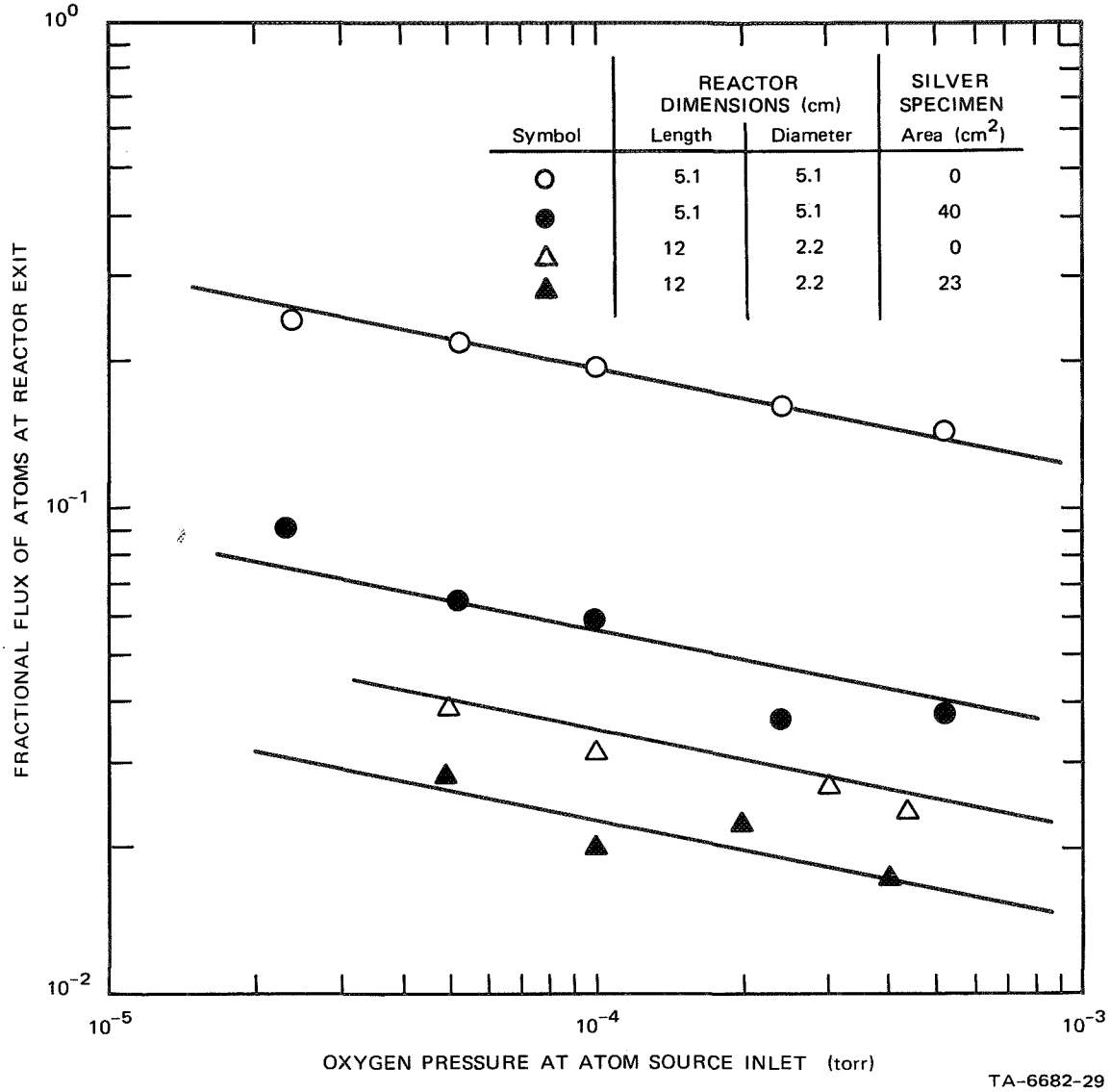

FIGURE 7 FRACTIONAL OXYGEN ATOM FLUX AT REACTOR EXIT AS A FUNCTION OF ATOM SOURCE PRESSURE AND REACTOR GEOMETRY. Source temperature T_W = 2125°K.

tric current through it, and the adsorbed gas was rapidly desorbed. This behavior was manifested as a pressure pulse detected by the mass spectrometer locked on the appropriate amu value. In accordance with established flash-filament experimental analysis,[8] the total mass of gas desorbed from the ribbon during the heating period was evaluated by integration of the pressure rise with respect to time. By observing the total mass of gas desorbed as a function of the time of exposure of the specimen at 300°K to the gaseous atoms, we could measure the rate of adsorption of atoms by the metal. The ratio of rate of adsorption to incident collision rate of atoms is termed the sticking coefficient S. Incident collision rates were computed from kinetic theory using the steady-state average number density of atoms in the reactor obtained from the measured exit flux and Eq. (15).

c. Atom Desorption Rate Measurements. When surface sorbed atoms were observed to desorb (as molecules) spontaneously from metal surfaces at room temperature, the process represented recombination of atoms by the Langmuir-Hinshelwood mechanism.[2] We measured the rate of this desorption by the following procedure. The specimen was first exposed to gaseous atoms for a sufficient length of time to ensure saturation coverage. The atom source was then cooled to a temperature at which thermal dissociation was negligible even though the total pressure in the system was not changed significantly. After a period of time, the metal ribbon was flash heated and the quantity of gas desorbed was determined. This procedure was repeated for a number of different dwell periods up to 90 minutes in duration.

d. The Behavior of Impurity Gases. Carbon monoxide was the major residual impurity in our vacuum system. This gas has been reported[9] to chemisorb strongly on some metals; hence we felt it important to evaluate the rate of sorption and the degree of coverage exhibited by carbon monoxide under the conditions of our experiments. The rate of coverage and sticking coefficient in the absence of atomic species were determined where possible in a manner identical to that employed for atoms.

In the case of hydrogen we observed a mass flux of water (amu 18)

in the reactor effluent as large as or larger than that of molecular hydrogen. The magnitude of this component diminished with time, presumably as the oxides that had accumulated in the atom source region were reduced by the atomic hydrogen. However, water remained a principal constituent in the effluent even after prolonged heating of a new tungsten ribbon in hydrogen at any temperature sufficient to dissociate hydrogen over our range of accessible hydrogen pressures. The presence of water was undesirable because it contributed substantially to the amu 1 peak due to cracking in the ion source of our mass spectrometer. The cracking pattern of water was determined over a range of pressures and of ionizing electron energies, but the contribution of amu 18 to amu 1 could never be reduced below 3%. This amount represented a sizable correction to apply to observed amu 1 amplitudes in all the experiments carried out in our apparatus.

IV. RESULTS AND DISCUSSION

A. Oxygen Atom Interactions

1. Gold

Measurement of the relative atom loss characteristics of gold (Table II) show that gold foil and electroplated gold behave similarly. Flash-filament experiments indicate that gold adsorbs up to a maximum of one monolayer of oxygen atoms at a finite rate at room temperature (Fig. 8). Molecular oxygen does not chemisorb on gold at a measurable rate at 300°K, but the sticking probability S of atomic oxygen on the clean surface has a value 0.044 (Fig. 9). The oxygen-covered gold exhibits a relatively low adatom-adatom (Langmuir-Hinshelwood) recombination rate at 300°K (Fig. 10), which cannot be attributed to displacement of oxygen adatoms by strongly bound CO (dashed curve in Fig. 10).

We conclude that the substantial atom removal capability indicated by $Q_O/Q_O^* = 0.2$ (Table II), occurs primarily by way of an Eley-Rideal (gas atom-adatom) recombination path. The value of Q_O/Q_O^* is independent of incident atom flux. This fact shows that the dominant removal rate is first order with respect to gaseous oxygen atoms, as must be the case for

Table II

RELATIVE OVERALL OXYGEN ATOM LOSS CHARACTERISTICS OF METALS

Specimen and Pretreatment	Q_O/Q_O^* (averaged values)[a]
Gold-foil ribbon	0.21
Electroplated gold film	0.20
Silver foil ribbon	0.61
Silver foil wall liner	0.61
Titanium foil ribbon, vacuum annealed	0
Titanium foil ribbon, preoxidized	0.67
302 Stainless steel (I), vacuum annealed at 800°C	0.15
302 Stainless steel (II), vacuum annealed at 400°C	0.06
Aluminum foil ribbon	1.0

[a] Fractional atom flow rate at exit of reactor of 12 cm length and 2.2 cm diameter. Asterisk represents empty reactor (no specimen).

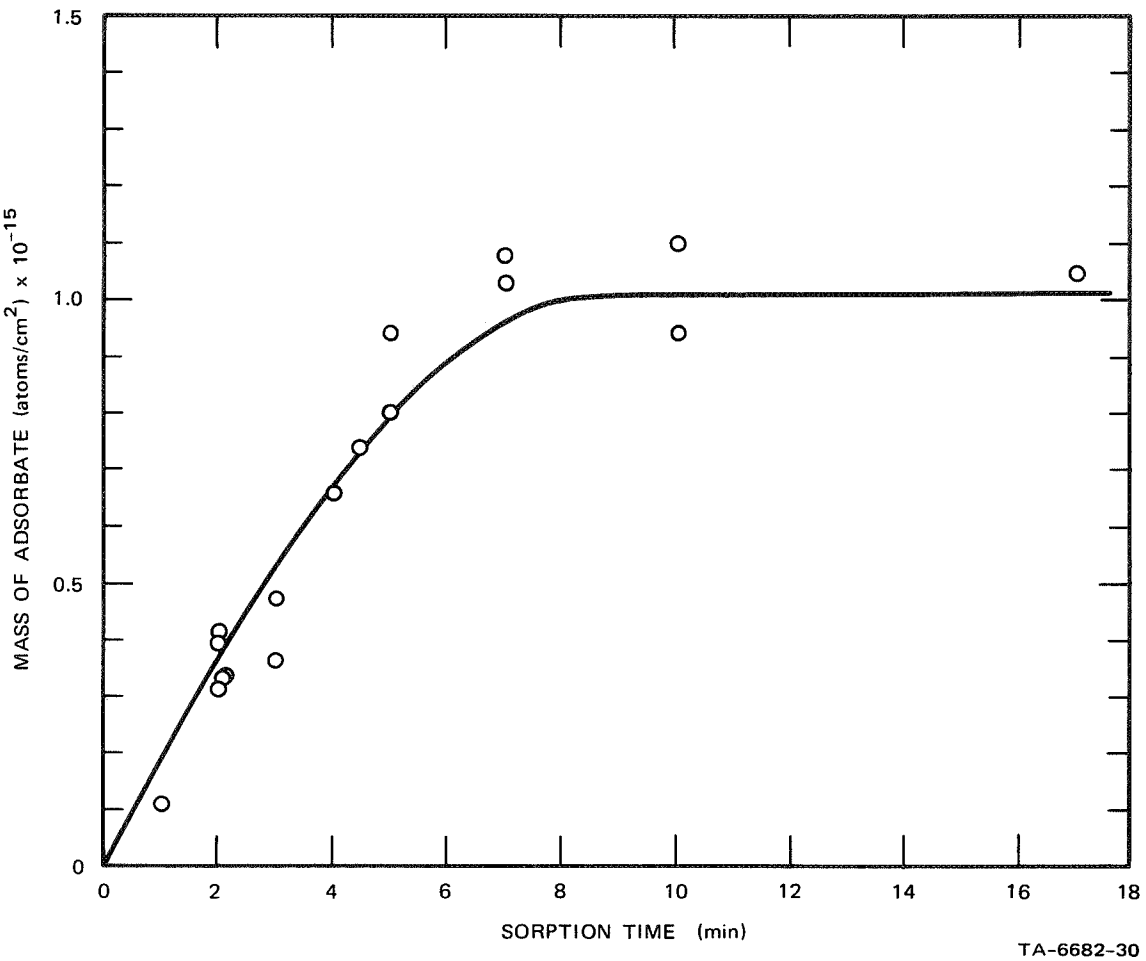

FIGURE 8 RATE OF ADSORPTION OF OXYGEN ATOMS ON GOLD AT 300°K. $P_o \cong 1.4 \times 10^{-7}$ torr.

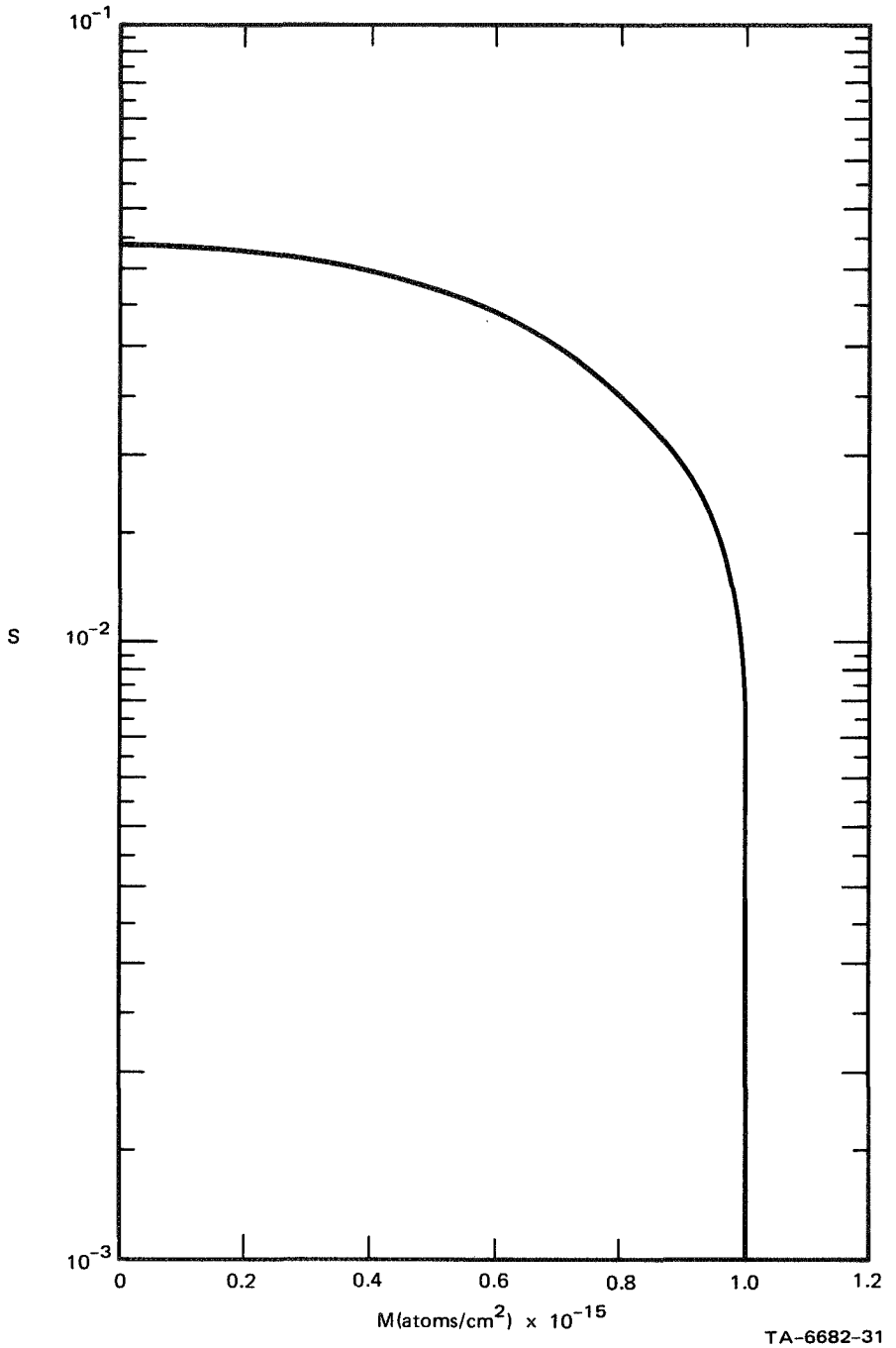

FIGURE 9 STICKING PROBABILITY S OF OXYGEN ATOMS ON GOLD AT 300°K AS A FUNCTION OF SURFACE COVERAGE M (CURVE DERIVED FROM DATA IN FIGURE 8).

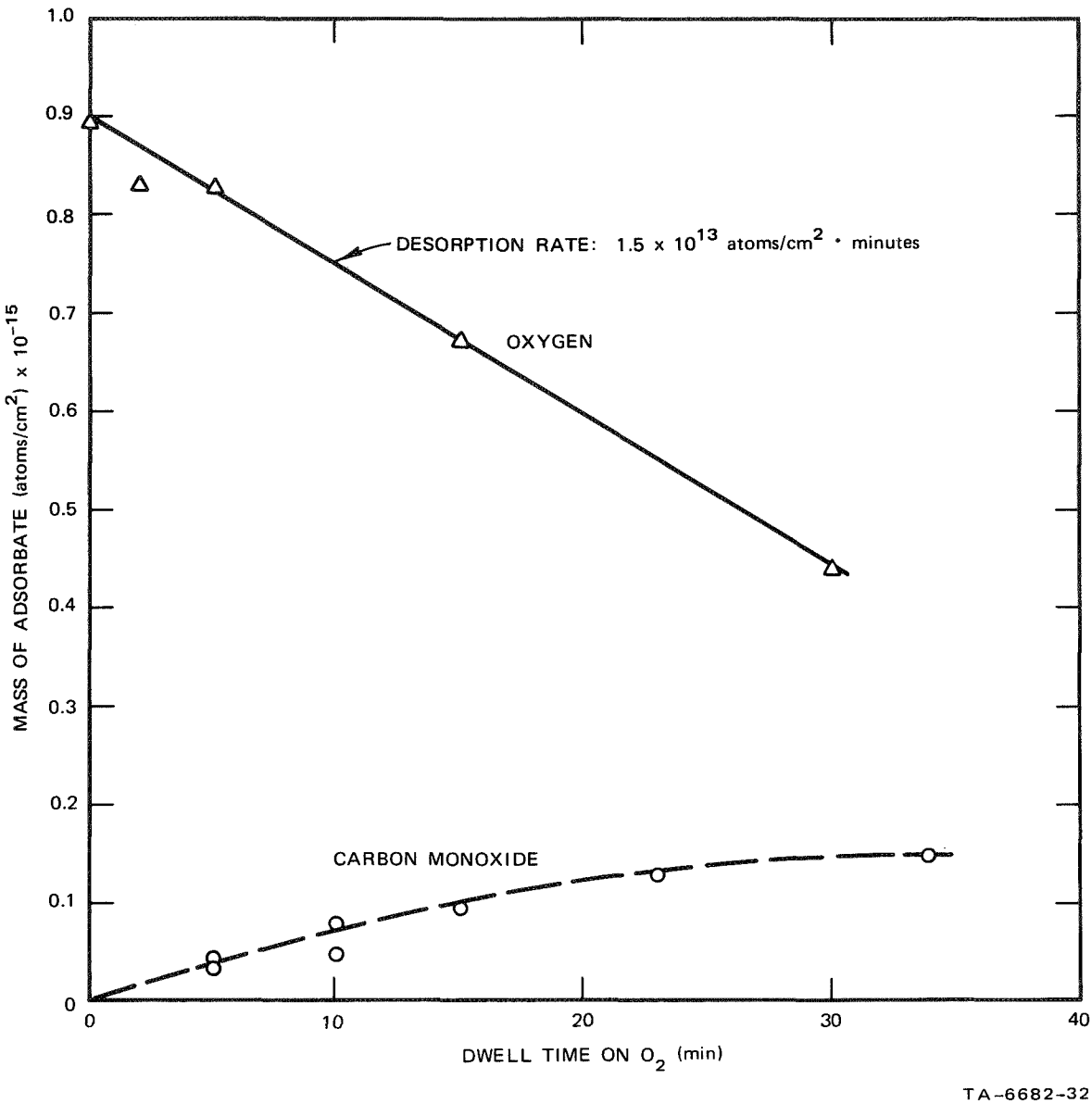

FIGURE 10 SPONTANEOUS DESORPTION OF OXYGEN FROM GOLD AT 300°K. At time = 0, gold surface was covered with approximately 1 x 10^{15} adatoms/cm^2. $P_{O_2} \cong 5 \times 10^{-5}$ torr. Rate of adsorption of CO is shown by dashed curve. $P_{CO} \cong 5 \times 10^{-6}$ torr.

an Eley-Rideal mechanism.

2. Silver

The total atom loss rate on silver is substantially less than that on gold (Table II). Flash-filament experiments show that at 300°K silver takes up atomic oxygen at a nearly constant rate well beyond monolayer coverage (Fig. 11), suggesting occlusion of the atomic species in the metal.

The rate of spontaneous desorption of oxygen from silver at 300°K was also investigated by means of the flash-heating technique. The results are shown in Fig. 7 as the difference between the amount of oxygen atoms sorbed during an exposure of ten minutes' duration to atomic oxygen (Fig. 11) and the amount recovered during the heating flash after the specified dwell period in molecular oxygen.

It is evident that most of the atomic oxygen occluded by the silver is bound with sufficient strength to be completely stable at 300°K (compare Figs. 11 and 12). A portion of the oxygen associated with the solid corresponding to the equivalent of less than one monolayer is not so strongly bound, however, and desorbs rather rapidly at 300°K.

The nature of the occluded state cannot be determined from our measurements. The rather prolonged constant rate of uptake of oxygen exhibited by our specimen (Fig. 11) suggests that the occlusion process is not hampered by the formation of a discrete phase in the form of a layer of some silver oxide. On the basis of available thermodynamic data,[10] both AgO and Ag_2O would be stable at 300°K in the partial pressure of oxygen atoms attained in our experiments. McBee and Yolken,[11] using an ellipsometric technique, noted that film growth on a silver surface exposed to an undetermined flux of oxygen atoms was nearly linear with time up to a thickness of over 1000 Å. Therefore, the formation of a surface oxide phase cannot be ruled out as the mechanism of occlusion in our experiments.

For the case of silver, we have total atom loss data from experiments in the short reactor ($L/R_o = 2$), which can be interpreted with our analytical model. The specimen was mounted in the reactor as a silver

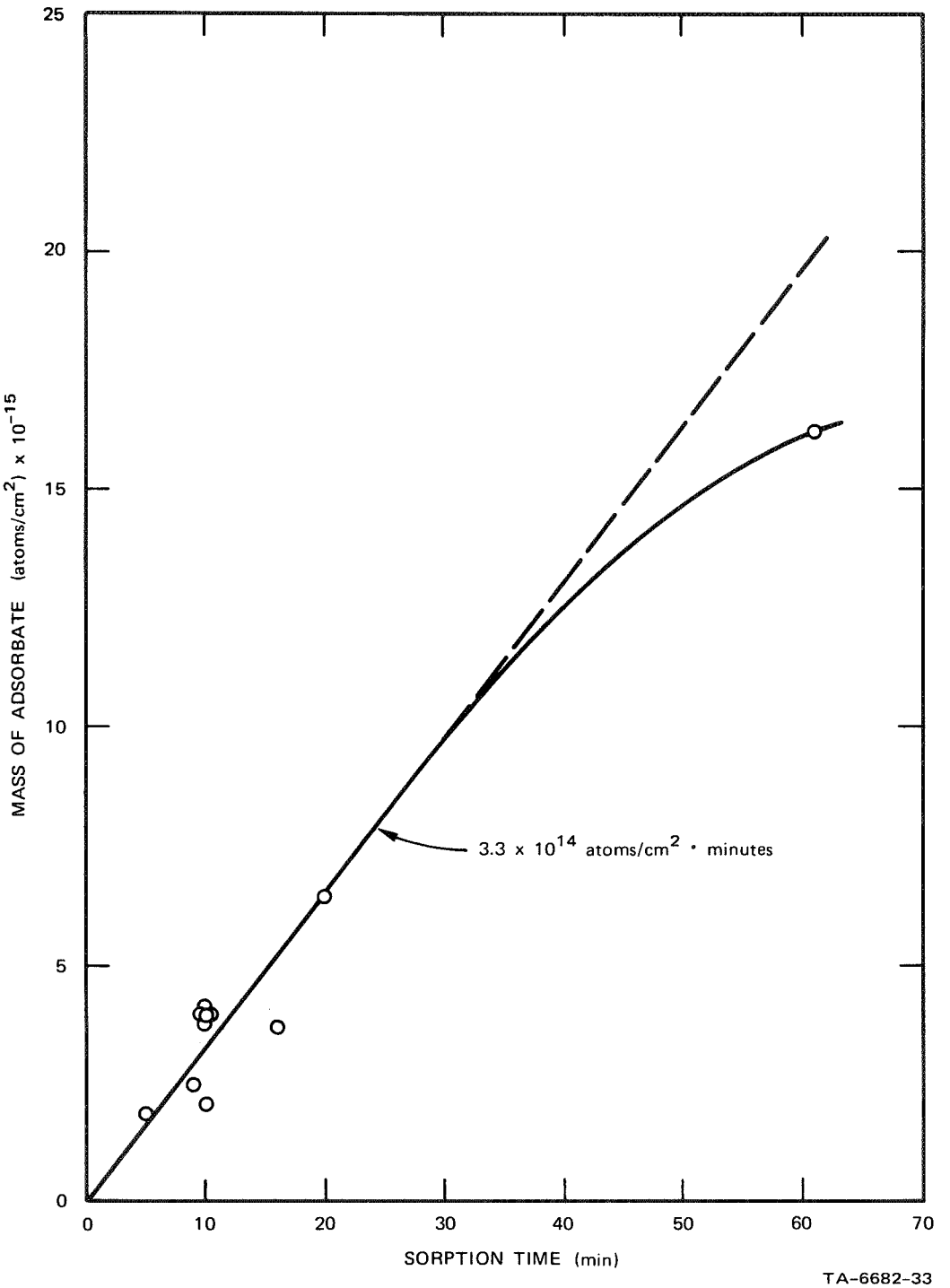

FIGURE 11 ADSORPTION/OCCLUSION OF OXYGEN ATOMS BY SILVER AT 300°K. $P_o \cong 1.4 \times 10^{-7}$ torr.

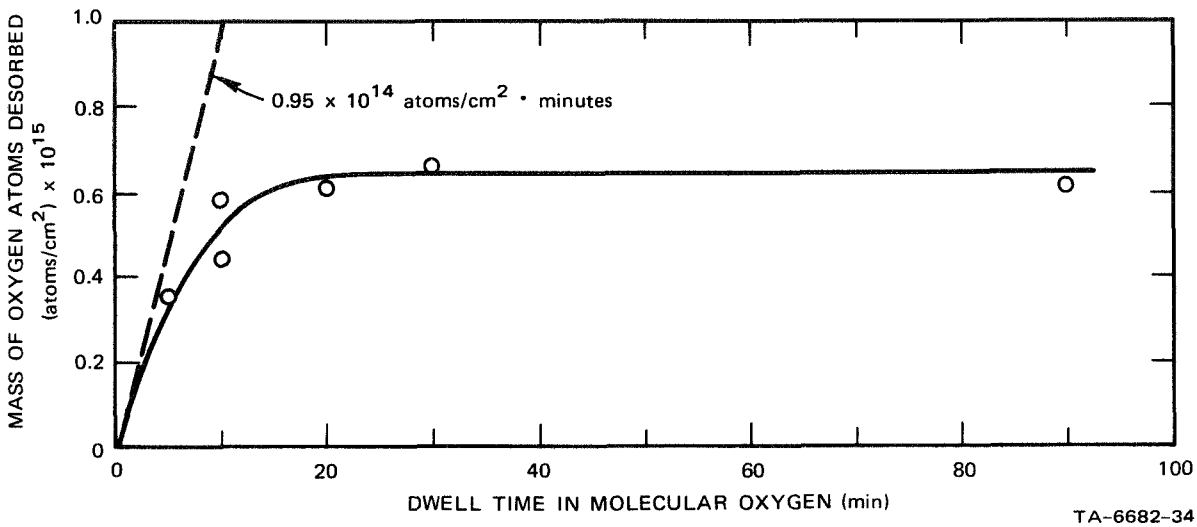

FIGURE 12 SPONTANEOUS DESORPTION OF OXYGEN FROM SILVER AT 300°K.
At time = 0, silver had been exposed to a constant flux of gaseous oxygen atoms ($P_o \cong 1.4 \times 10^{-7}$ torr) for 10 minutes. $P_{o_2} \cong 2 \times 10^{-5}$ torr).

foil liner, which covered exactly one-half the side wall of the reactor nearest the end containing the exit aperture (similar to the geometry depicted in Fig. 4). This liner was cut from 0.010-in. silver foil, polished with a pure alumina abrasive, and washed thoroughly in distilled water. Rolled into a cylinder of slightly larger diameter than the reactor, it was held in place by spring tension. After evacuation, the silver was initially degassed by heating to approximately 300°C with a resistance heater surrounding the quartz reactor. Silver was chosen for this experiment because of its demonstrated[12] indifference to CO as a catalytic poision for oxygen-surface reactions. Consequently, we could be confident that it would exhibit its characteristic steady-state activity toward atomic oxygen without periodic flash cleaning.

These experiments (Fig. 13) demonstrate a reasonably constant fractional diminution in the flux of oxygen atoms that survive transit through the reactor with the silver wall, over a range of source temperatures and pressures. The analytical model permits interpretation of this fractional loss in terms of a loss coefficient, α_{band}. The average observed value of relative exit flux, $Q/Q^* = 0.31$, corresponds to an overall loss coefficient, $\alpha_{band} \cong 0.1$ (Fig. 6, curve b), according to the analytical model.

The magnitude of this parameter is comparable to the ratio of the combined measured rates of occlusion (3.3×10^{14} atoms/cm^{2}min) and Langmuir-Hinshelwood recombination (1×10^{14} atoms/cm^{2}min), to the rate of impingement of gaseous atoms (4.3×10^{15} atoms/cm^2 min). These observations lead us to conclude that the rate of recombination by way of an Eley-Rideal path is small, and that occlusion/chemical reaction is the major mode for gaseous atom loss on silver. It seems probable that the high values of recombination efficiency reported by others[2] may in reality represent a combined reaction efficiency for recombination and occlusion.

The fractional atom flow rate Q_O/Q_O^* at the exit of the long reactor (Table II) is about a factor of 3 higher for silver than for gold. Yet the Langmuir-Hinshelwood rate of recombination is nearly a factor

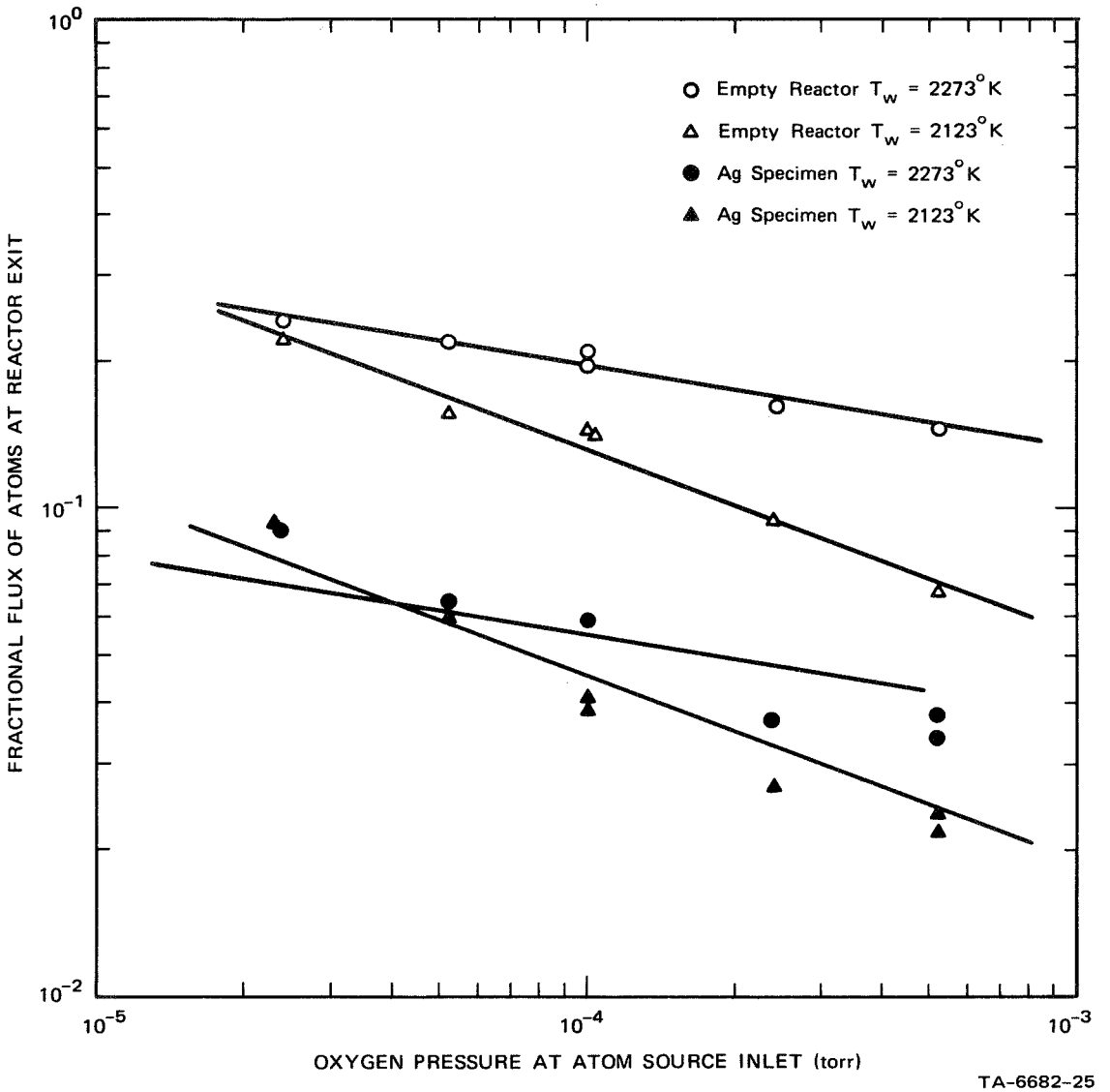

FIGURE 13 FRACTIONAL OXYGEN ATOM FLUX AT REACTOR EXIT AS A FUNCTION OF ATOM SOURCE TEMPERATURE, T_W, AND PRESSURE.

of 10 lower for gold (Fig. 10) than for silver (Fig. 12). In addition, gold exhibits no occlusion of atomic oxygen nor gives any evidence of oxide formation. Consequently, we conclude that atom loss occurs on gold primarily by an Eley-Rideal mechanism at a rate approximately three times faster than the rate of occlusion of oxygen by silver, viz., 1×10^{15} atoms/cm^{2}min. This difference could be attributed to a chemisorbed oxygen state on gold with a greater binding energy than that on silver. The stronger binding energy for gold provides an oxygen adatom population with relatively low mobility, thus ensuring a high probability for gas atom-adatom collision. On silver the sorbed atoms are highly mobile, residing for very brief periods on any one site so that a very low fraction of the incident atoms encounters adatoms.

3. Titanium

Before exposing the titanium specimen to atomic oxygen, the ribbon was annealed at temperatures up to 1173°K and degassed under high vacuum conditions. During this treatment large quantities of hydrogen and water were observed flowing out of the reactor. CO and CO_2 were also noted but in considerably smaller quantities (less than 1% of the hydrogen). Upon continued heating at 823°K, the water, CO, and CO_2 diminished quite rapidly relative to the hydrogen, which required several hours to reduce to less than 10% of its original value.

Following this treatment, the ribbon, at 300°K, was exposed to a flux of atomic oxygen from the tungsten ribbon source at the reactor inlet. No flux of oxygen atoms was observed at the reactor outlet, and this situation persisted during the approximately hour-long duration of this experiment (Table III).

After the reactor was evacuated to base pressure ($\sim 10^{-9}$ torr), the specimen was heated to 1023°K. As before, water and hydrogen were the major components liberated; no atomic oxygen was observed.

The specimen was then deliberately oxidized by heating to 1023°K in molecular oxygen at $P \cong 10^{-6}$ torr for a period of 105 minutes. During this time the steady-state oxygen pressure diminished, rapidly at first, then more slowly. When the ribbon was cooled, the oxygen pressure rose

Table III

EFFECT OF TITANIUM SPECIMEN ON
GAS COMPOSITION AT REACTOR OUTLET

Specimen		Mass Flow Rate[a] at Reactor Outlet (torr-ℓ/sec) x 10^6	
Temperature (^{0}K)	Pretreatment	O	O_2
300	Vacuum Anneal	0	22.7
300	Oxidation	0.615	21.2
773	Oxidation	0.27	4.2
Empty Reactor		0.98	21.3

[a] Steady-state values obtained with inlet pressure 1 x 10^{-4} torr and atom source at 2273^{0}K. All values for O corrected for mass spectrometer cracking factor.

to its original value within a few minutes. The specimen exhibited no dramatic change in appearance; it was still a satin silvery grey.

A repeat of the atomic oxygen exposure experiment now gave significantly different results. A substantial fraction of the incident atomic oxygen appeared at the outlet of the reactor (Table III). When the specimen was heated under these conditions, the picture changed dramatically (Fig. 14). At a specimen temperature of 773°K, both atomic and molecular oxygen diminish but the former much less so than the latter. The molecular oxygen reaction rate changes with time in such a way that the pressure of oxygen increases until a new steady state is attained. Cooling the titanium restores the molecular oxygen nearly to its original pressure, but the atomic oxygen pressure remains at a reduced value (Fig. 14).

Finally a subsequent experiment carried out in pure molecular oxygen showed no change in the ratio amu 16/amu 32 with titanium specimen temperature, and very little affinity for molecular oxygen. However, the ribbon had now acquired a distinct blue coloration, presumably an oxide film of some thickness.

The behavior of titanium in the presence of atomic and molecular oxygen is complex. It seems likely that the complexity may be related to variations in the surface composition of the specimen. At least four oxides of titanium, viz., TiO, Ti_2O_3, Ti_3O_5, and TiO_2, have been characterized and are known to be highly stable compounds, even at molecular oxygen pressures less than 10^{-8} torr. In addition, there undoubtedly exist nonstoichiometric titanium-oxygen combinations, which may exhibit varying degrees of stability relative to the stoichiometric oxides. In one study[13] it was established that titanium reacted initially with oxygen at low pressures by dissolution of the gas into the metal lattice. The rather dramatic initial enhancement in the affinity of the metal for molecular oxygen versus atomic oxygen upon heating (Fig. 14) may be caused by a significant difference in the energies of activation for molecular oxygen dissolution compared to atomic oxygen dissolution. The activation energy value for the former process has been reported[13] to be 22 kcal/mole, whereas one would expect the latter process to be vir-

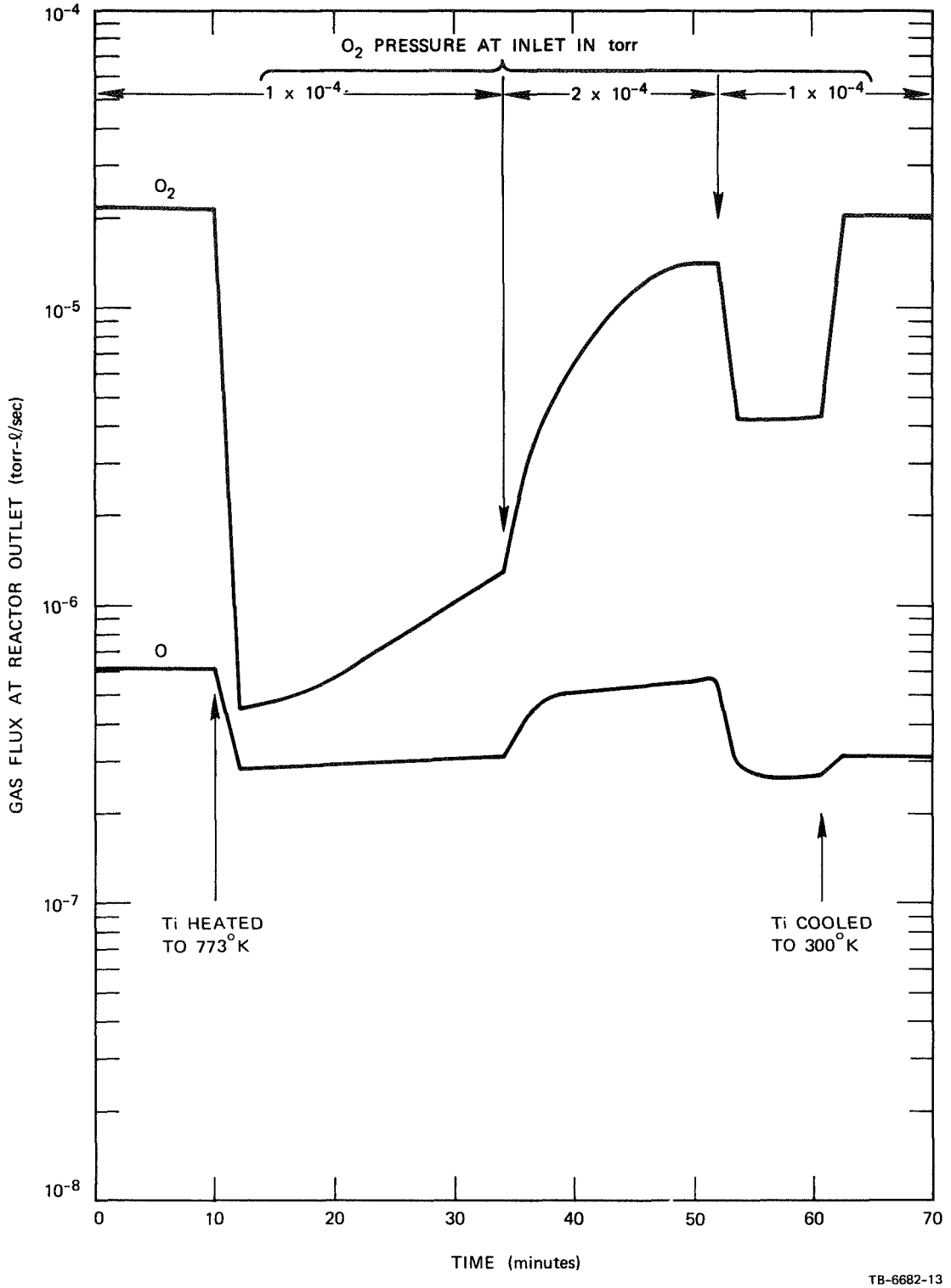

FIGURE 14 EFFECT OF TITANIUM SPECIMEN TEMPERATURE ON GAS COMPOSITION AT REACTOR OUTLET.

tually nonactivated.[2] Hence, though the rate of interaction of titanium with molecular oxygen may be substantially slower than with atomic oxygen at 300°K, the situation may be reversed at 773°K. Also the high concentration of molecular oxygen relative to atomic oxygen contributes to the observed difference in reaction rate.

The high reactivity of the vacuum annealed specimen for atomic oxygen we attribute to a relatively clean metallic surface. The appearance of water and hydrogen during the annealing process suggests that oxides on the surface may have been reduced by this treatment, leaving clean titanium with a very high affinity for atomic oxygen. Conceivably, long exposure of this surface to the atomic oxygen atmosphere would have passivated it.

4. Stainless Steel

We prepared two specimens of type 302 stainless steel foil, each cut in the shape of a narrow ribbon with a geometric surface area of 23 cm^2. Type 302 is a general purpose, low-carbon stainless steel widely used for fabrication of vacuum system components.

One ribbon (designated I) was vacuum annealed at 1073°K. Initially, copious quantities of gas (mainly H_2O and CO) were liberated from the heated ribbon. After a few minutes at annealing temperature, the ribbon acquired a mottled appearance. Upon cooling, the ribbon's original satin silver sheen had given way to a blue-brown transparent discoloration. In addition, a transparent black deposit appeared on the inside wall of the reactor.

The flux of surviving oxygen atoms with specimen I in the reactor, relative to that observed without a specimen, averaged 15% (Table II). During one experiment with this specimen, nitrogen was added to the inlet oxygen supply so that up to 20% of the gas flowing into the reactor was nitrogen. However, there was no evidence of NO (mass 30) or NO_2 (mass 44) formation, nor was there any appearance of nitrogen atoms (mass 14) above the background produced in the mass spectrometer ion source.

Specimen I was removed from the reactor and the survival of oxy-

gen atoms was again measured in the presence of the black deposit on the reactor wall. The value of flux observed was in good agreement with that obtained under identical conditions before specimen I had been mounted in the reactor, indicating that the deposit on the reactor wall was quite inert to chemical or catalytic interactions with oxygen atoms.

The apparatus was disassembled and the interior of the reactor thoroughly cleaned. Specimen II was then mounted in the reactor and degassed under considerably less severe conditions than those employed for specimen I. The stainless steel ribbon was heated to 673°K for one-half hour. As with the previous specimen, large quantities of CO and H_2O desorbed, but in this case no discoloration of the specimen occurred and no deposit appeared on the reactor wall.

The fractional surviving flux of oxygen atoms was even lower with specimen II than with specimen I, averaging 6% (Table II). In this case, however, examination of the mass spectrograms showed an unusually large quantity of CO_2 in the reactor effluent. The observed variation of net CO_2 flux with oxygen atom flux in one set of experiments is shown in Fig. 15.

It is apparent that the stainless steel specimens employed in our experiments are efficient sinks for atomic oxygen relative to the noble metals, gold and silver, and to preoxidized titanium, irrespective of annealing temperature. However, the mechanism of atom loss on the steel surface seems to be different for the specimens annealed at different temperatures. On the surface annealed at 1073°K, the oxygen atoms are removed either by occlusion or by recombination, whereas they appear to react with carbon in some form on the surface of the specimen annealed at 673°K to form CO_2. The stoichiometry of such a reaction requires the combination of two oxygen atoms with one carbon atom to form one molecule of CO_2. Consequently, if all the available atomic oxygen were to react with surface carbon, one would expect a CO_2 flux equal to one-half the incident oxygen atom flux. The data suggest that such a mass balance does obtain. In Fig. 16 smooth curves are drawn through the data points for the CO_2 flux and one-half the oxygen atom flux observed in the effluent of the empty reactor as the total molecular oxygen flux through the

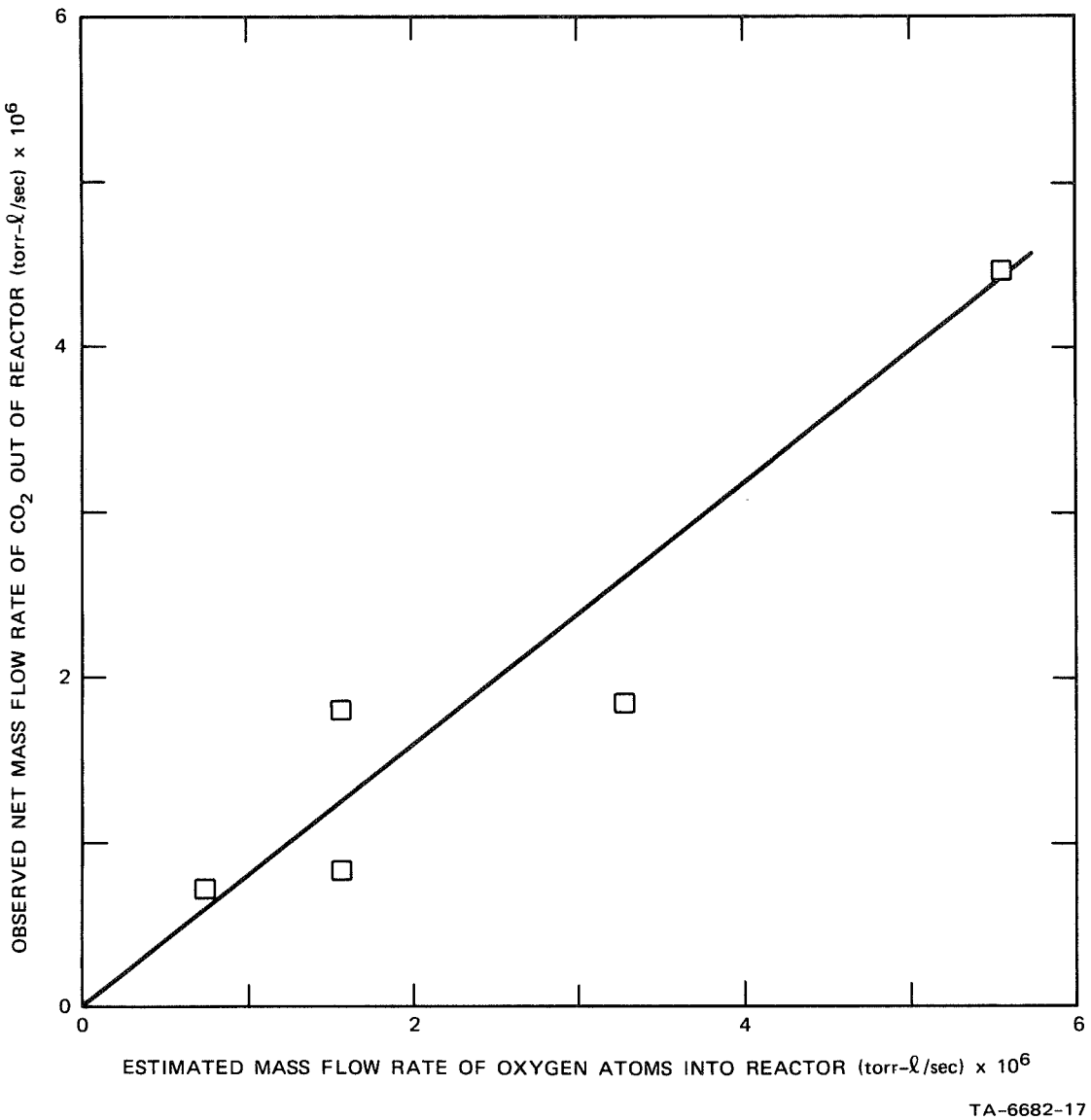

FIGURE 15 CO_2 FLOW RATE AS A FUNCTION OF MASS FLOW RATE OF OXYGEN ATOMS INTO THE REACTOR. Atom flow rates estimated from data obtained with empty reactor.

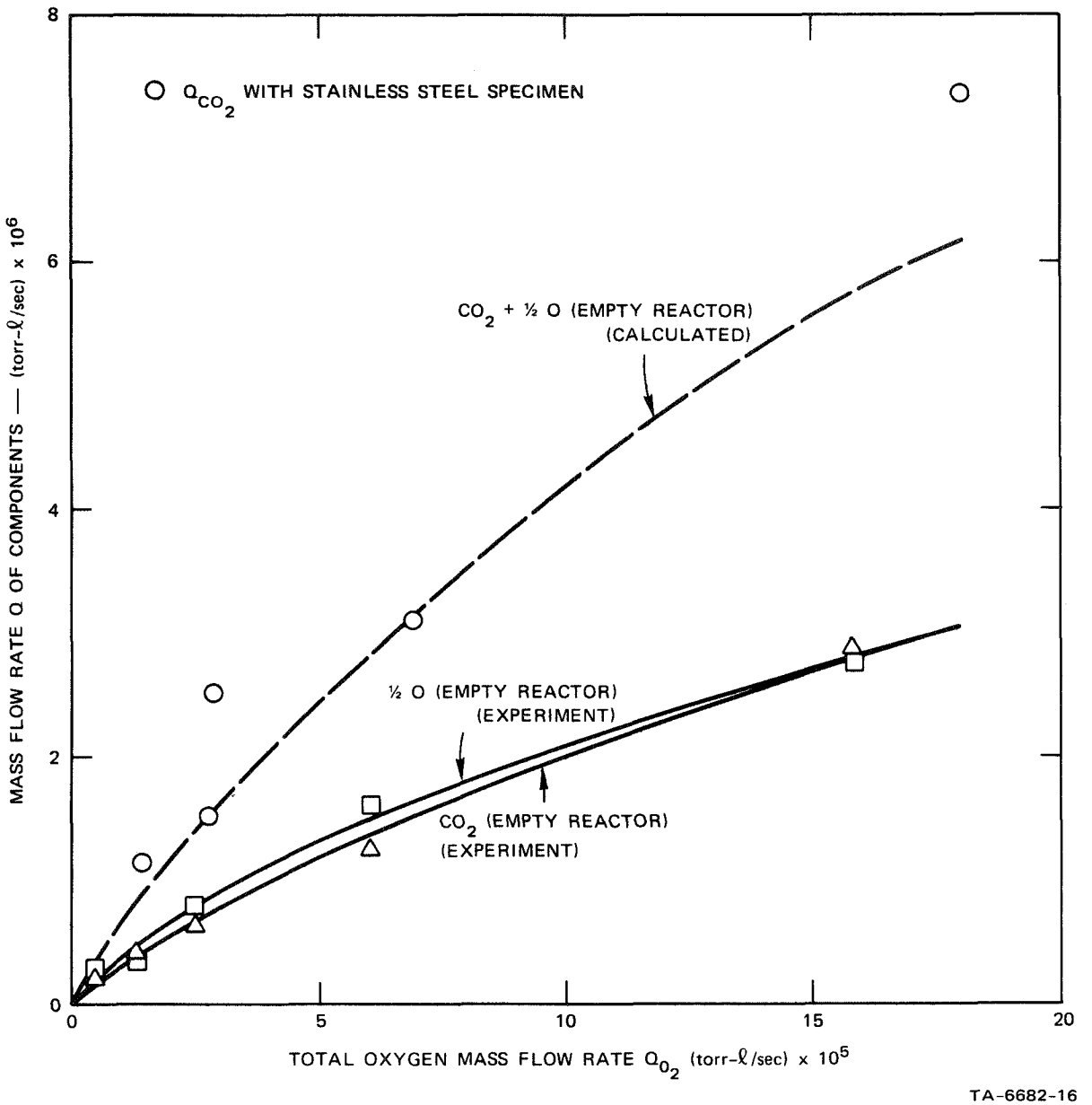

FIGURE 16 MASS FLOW RATE OF ATOMIC OXYGEN AND CARBON DIOXIDE FROM REACTOR WITH AND WITHOUT STAINLESS STEEL SPECIMEN AT 300°K. Atom source temperature: 2275°K.

reactor is increased. These curves represent, respectively, the baseline residual CO_2 in the reactor effluent, and one-half of the available incident flux of oxygen atoms in the reactor under the specified conditions of tungsten ribbon temperature and molecular oxygen throughput. The sum of these curves (dashed curve in Fig. 16) represents the resultant CO_2 flux if all of the incident oxygen atoms react to form CO_2. The agreement between this curve and the observed CO_2 data points (open circles) suggests strongly that this is the fate of the atomic oxygen in this case.

Why the simple differential in annealing temperature imparted such different surface characteristics to the two specimens is an open question. Type 302 stainless steel contains a maximum of 0.15% carbon which is normally combined with the iron and chromium as carbides in a homogeneous solid solution (austenite).[14] At temperatures greater than 773°K, the solubility of these carbides diminishes and they precipitate along grain boundaries. Hence, a stainless steel specimen annealed at 1073°K would possess a different surface structure with respect to carbon distribution than one annealed at 673°K. In view of the complexity of these solid phases, we feel that further speculation on a mechanism of interaction is without merit.

It is interesting to compare the oxygen atom loss characteristics of stainless steel specimens in our laboratory apparatus with those observed by Kasprzak, Krankowsky, and Nier[15] in the upper atmosphere. These investigators sent aloft on an Aerobee rocket two mass spectrometers; one with an exposed ion source (termed "open source") and a second with an ion source situated at the bottom of a cavity connected to the ambient atmosphere through a cylindrical stainless steel tube (termed "closed source"). The linear distance from the tube aperture to the ion source was approximately 5 inches, but the geometry was complex.[16] Amu 16 data obtained during this flight showed that only about 5% of the atomic oxygen reported by the open source spectrometer was seen by the closed source instrument, indicating a substantial loss of atoms on the wall of the antechamber. Based on an analysis that assumed a uniform collision density of atoms on the antechamber wall, these authors suggest that the

stainless steel surface possesses a loss coefficient of 0.14. In view of the complexity of the geometry, we feel the numerical accuracy of this value is uncertain. However, the observed loss of oxygen atoms in the closed source instrument is unequivocal, and the magnitude of the loss is not in disagreement with the results of our experiments.

Furthermore, the nearly identical values of molecular oxygen number density reported by the two spectrometers in this flight indicate that the mechanism of atom loss on the stainless steel surfaces was not by catalytic recombination. Kasprzak[15] stated that there seemed to be no clear relationship between the observed number densities of atomic oxygen and CO_2, but data obtained in an earlier, similar flight by Nier and his associates[17] show that the amu 44 peak was nearly proportional to the amu 16 peak. Such a relationship was cited by von Zahn[1] from the data of other investigators also. In the light of evidence from both flight and laboratory data, we conclude that chemical reaction with carbon in some form on the surface may be a significant pathway for oxygen atom removal by stainless steel. It is of interest to note in this respect, that Marsh and his associates[18] measured the reaction rate of gaseous atomic oxygen with graphite and other carbons at room temperature and observed both CO and CO_2 as primary products.

5. Aluminum

Reports of a number of investigators[2,19] that aluminum possesses a very low catalytic activity for oxygen atom recombination led us to examine the atom loss characteristics of this metal. We cut a specimen from 0.001-inch thick, commercial foil, obtained from the Aluminum Corporation of America.

Before exposure to oxygen atoms, the specimen was heated in vacuum to remove adsorbed contaminants. Aluminum melts at 933°K; hence the cleaning operation had to be carried out at a very modest temperature. We maintained the specimen at 523°K for about 30 minutes; during this time water vapor was the main contaminant that desorbed from the surface.

Following this treatment of the specimen, oxygen was admitted to the system and the tungsten source was heated to 2273°K to generate oxy-

gen atoms. The composition of the reactor effluent was monitored as a function of oxygen pressure at the inlet to the atom source region, and of temperature of the tungsten source. The observed efflux of atomic oxygen was identical to that observed in complementary experiments with no specimen in the reactor, within the limits of experimental error.

After the aluminum specimen had been exposed to gaseous oxygen atoms for more than one hour at room temperature, it was heated to 523°K for several minutes. This procedure caused no pressure pulse in the reactor that could be attributed to the desorption of oxygen or any other gas.

The aluminum specimen employed in our experiments had been stored and manipulated in air before insertion into our vacuum system. Consequently, the surface was undoubtedly covered with a layer of aluminum oxide of undetermined thickness. This oxide is extremely stable, and could not be expected to dissociate or vaporize in the high vacuum environment during the mild (523°K) cleaning treatment that we used. We conclude that the inert character of this surface toward oxygen atoms must be attributed to aluminum oxide. The lack of recombination activity observed in our experiments is quite consistent with the reported[2] low values of oxygen atom recombination efficiency for aluminum oxide determined in higher pressure experiments.

B. Hydrogen Atom Interactions

1. Gold

The desire to evaluate quantitatively the upper atmosphere particle density of hydrogen atoms from amu 1 peak amplitudes reported by the OGO-F satellite mass spectrometer, led us to an investigation of the interaction of hydrogen atoms with gold. Molecular hydrogen can be thermally dissociated; in fact, the dissociation process on a heated tungsten ribbon has been studied.[20] We chose, therefore, to employ the identical atom source used for oxygen in our experiments as a source for hydrogen atoms.

Our apparatus was modified only by addition of a hydrogen inlet line and valve, in parallel with the existing oxygen inlet line. Experi-

ments were then carried out in a manner analogous to those using oxygen; that is, the hydrogen inlet valve was opened to establish a steady-state flow through the apparatus while the tungsten ribbon was heated to 2173°K, and the composition of the reactor effluent was monitored with the mass spectrometer. Specifically, we observed the ratio of atomic to molecular hydrogen (amu 1/amu 2) as a function of the pressure of hydrogen in the atom source inlet.

The surviving flux of hydrogen atoms, even with no specimen in the reactor, was quite small. The data (Table IV) show, however, that the magnitude of the surviving atom flux is significantly diminished when the gold specimen is situated in the reactor. This specimen is the identical piece of 0.002-inch foil, with a geometric surface area of 24.5 cm^2, employed in our earlier measurements with atomic oxygen. The observed fractional change in surviving flux of hydrogen atoms, Q_H/Q_H^*, has a value of 0.62 (the asterisk represents the quantity associated with the empty reactor).

Our first measurement of the rate of adsorption of atomic hydrogen on gold indicated the saturation coverage to be well below 0.1 monolayer. This value seemed insufficient to account for the observed total loss of atoms on the gold surface; hence we performed additional experiments to investigate the dependence of the surface kinetics on atomic hydrogen pressure and coverage.

We varied the atom partial pressure by changing the total hydrogen flux through the reactor. This change affects both atomic and molecular hydrogen pressures in the reactor, but the rate of adsorption of molecular hydrogen on gold is negligibly small at the temperature of our experiment (300°K). The results of these experiments (Fig. 17) show the steady-state surface coverage increases with the pressure of atomic hydrogen. The initial rate of adsorption on clean gold, however, seems to be first order with respect to atom pressure within the precision of our pressure measurements. Hence, the value of the sticking coefficient S remains constant with atom pressure at low surface coverages (Fig. 18).

We also measured the rate of desorption of hydrogen (as molecules)

Table IV

SURVIVING FLUX OF HYDROGEN ATOMS

Specimen	Atom Source Temperature (^{o}K)	Atom Flow Rate at Reactor Outlet Relative to Hydrogen Molecules (Q_H/Q_{H^2}) [a]
None	1973	0.0023
None	2173	0.0055
Gold [b]	2173	0.0034

[a] Average values from a number of experiments at various total flow rates, corrected for contribution from water (amu 18).

[b] Foil ribbon, geometric surface area 24.5 cm^2.

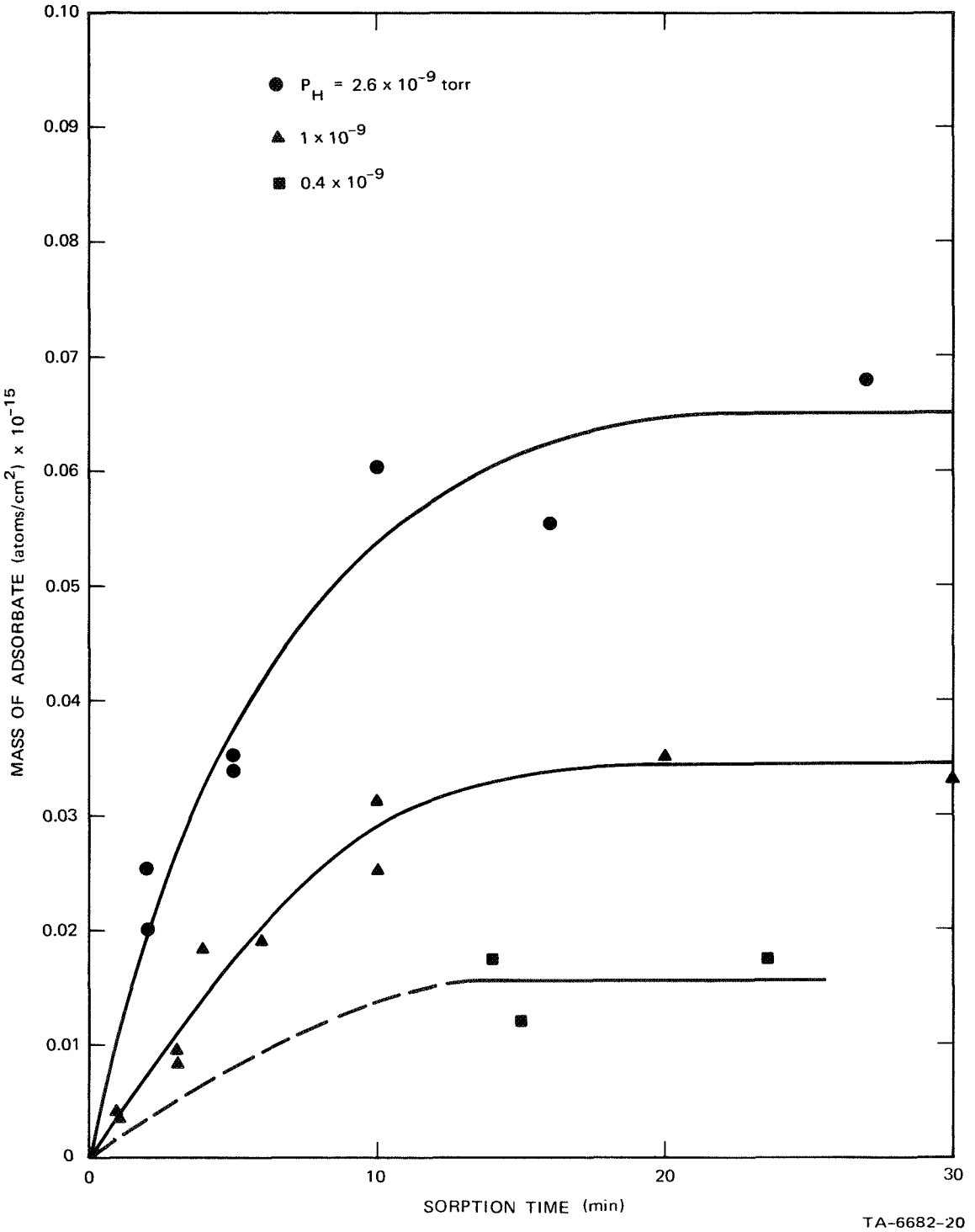

FIGURE 17 THE ADSORPTION OF ATOMIC HYDROGEN ON GOLD AT 300°K AS A FUNCTION OF PRESSURE.

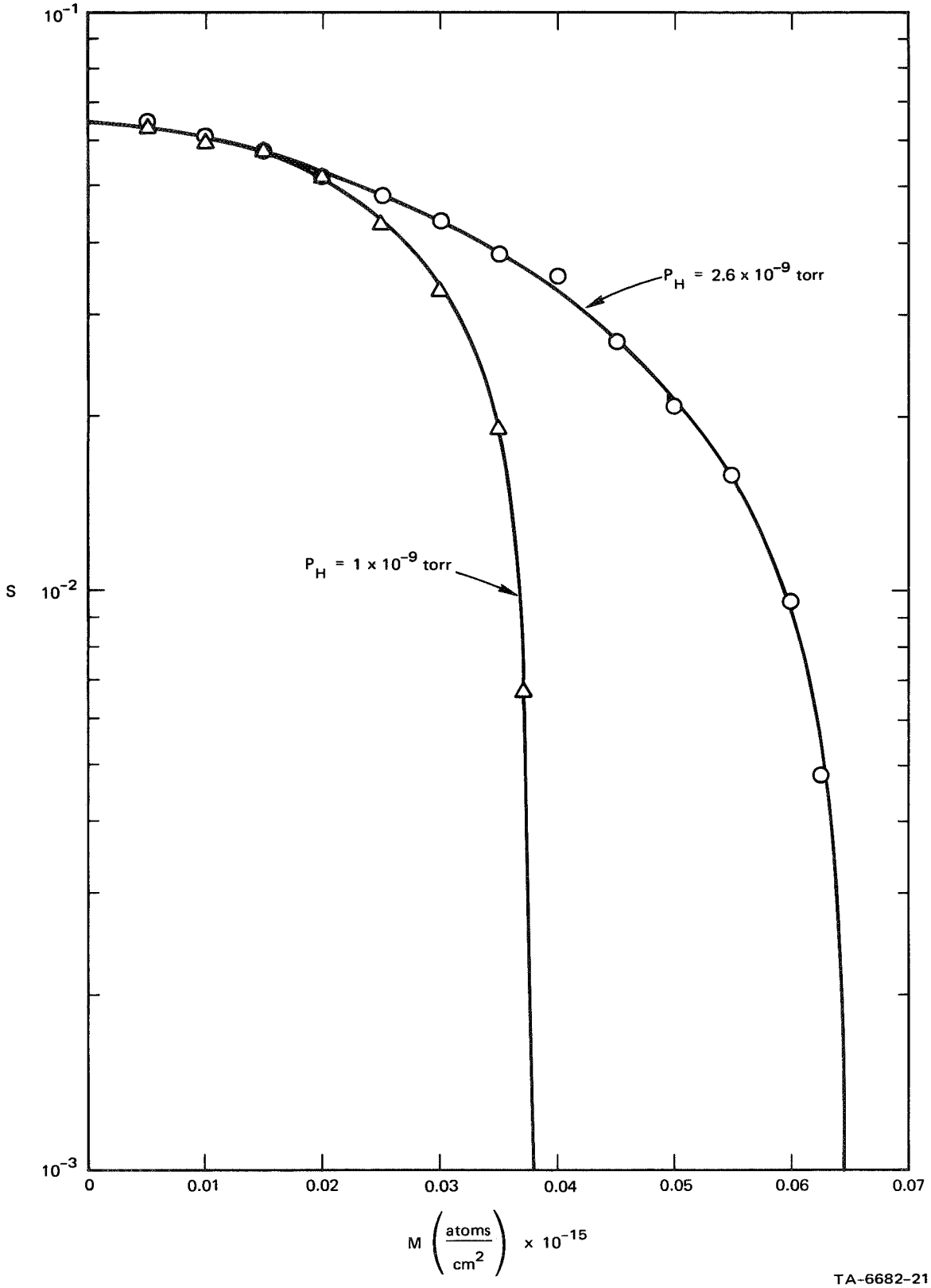

FIGURE 18 STICKING COEFFICIENT S OF ATOMIC HYDROGEN ON GOLD AT 300°K AS A FUNCTION OF SURFACE COVERAGE OF ADATOMS M. Points are normalized to coincide at M = 0 within precision of pressure measurements.

from gold. The observed rate (Fig. 19) from an initial coverage of 0.016×10^{15} atoms/cm^2 is about a factor of 10 lower than the clean-surface adsorption rate at an atomic hydrogen pressure which gives this steady-state coverage (compare with Fig. 17).

The observed characteristics of the atomic hydrogen-gold system can be interpreted in terms of the kinetics of three elementary processes[2] occurring at the surface. The following list associates these processes with methematical expressions relating the rate of population or depopulation of hydrogen on the surface to the concentration of gaseous atoms n, the surface number density of available adsorption sites N, and the fraction of sites occupied by adatoms θ.

Sorption $\quad H(g)+(s) \xrightarrow{k_1} H(s) \quad \frac{d[H(s)]}{dt} = k_1 N(1-\theta)n \quad (16)$

Recombination:
Langmuir-Hinshelwood $\quad H(s)+H(s) \xrightarrow{k_2} H_2(g)+2(s) \quad \frac{-d[H(s)]}{dt} = k_2(N\theta)^2 \quad (17)$

Recombination:
Eley-Rideal $\quad H(s)+H(g) \xrightarrow{k_3} H_2(g)+(s) \quad \frac{-d[H(s)]}{dt} = k_3 N\theta n \quad (18)$

Based on equilibrium data, the probability of atom desorption from gold is virtually nil, so we need not consider the reverse of reaction (16). In addition, under the conditions of our experiments, we do not observe sorption of hydrogen from the molecular state; hence, the reverse of reactions (17) and (18) is eliminated from our consideration.

Using these elementary steps and assuming a mass balance in a dynamic steady state, we can equate the rate of sorption to the combined rates of recombination:

$$k_1 N(1-\theta)n = k_2 (N\theta)^2 + k_3 N\theta n \quad (19)$$

Rearrangement of Eq. (19) gives a statement of the functional dependence of θ on n:

$$n = \frac{k_2 N\theta^2}{k_1(1-\theta)-k_3\theta} \quad (20)$$

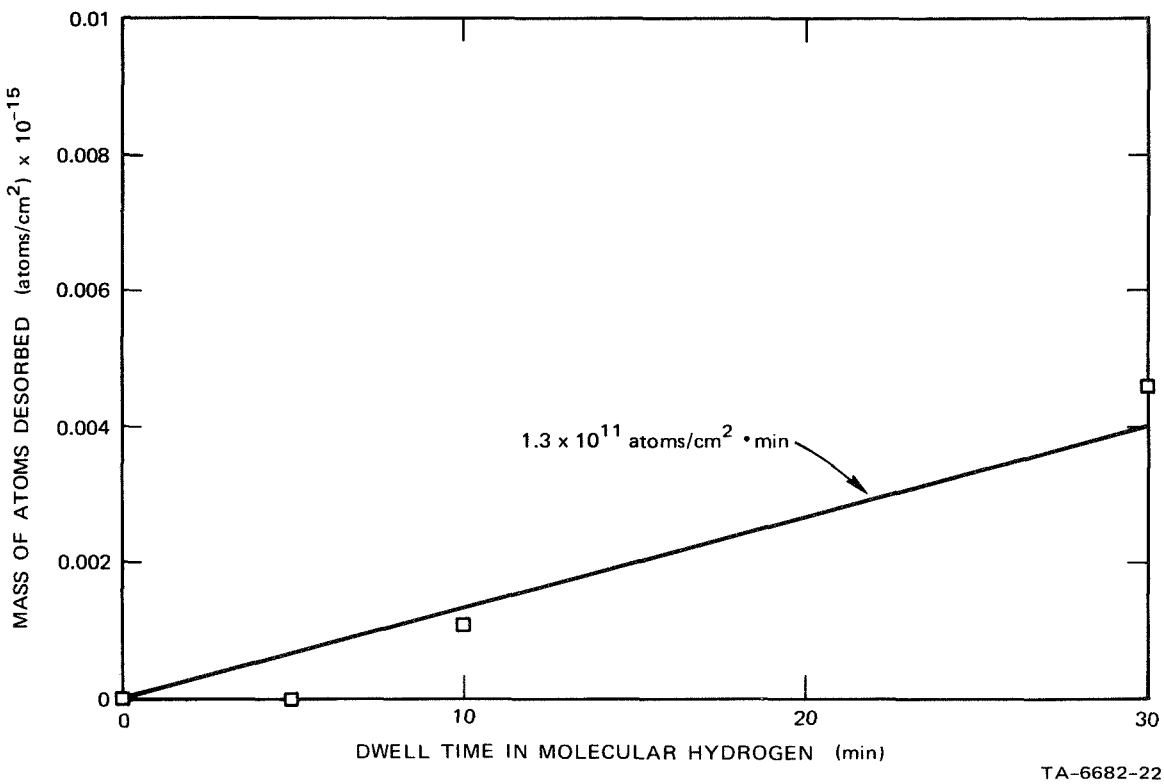

FIGURE 19 SPONTANEOUS DESORPTION OF HYDROGEN ADATOMS FROM GOLD AT 300°K. Initial coverage at time 0 = 0.016 x 10^{15} atoms/cm^2.

The reaction rate constants (k_1, k_2, k_3) in Eq. (20) may be evaluated from our experimental rate data:

k_1, computed from data in Fig. 17 using Eq. (16) = 1.25×10^{-10} $(atoms/cm^3)^{-1}min^{-1}$;

k_2, obtained for the observed coverage from data in Fig. 19, using Eq. (17) = 5.1×10^{-16} $(atoms/cm^2)^{-1}min^{-1}$;

k_3, obtained from Eq. (18), first computing the value of $k_3N\theta n$, for the observed coverage using Eq. (19) = 7.2×10^{-9} $(atoms/cm^3)^{-1}$ min^{-1}.

The adsorption isotherm (θ vs n) obtained by solving Eq. (20) using these values of the rate constants, predicts a maximum steady-state surface coverage less than 0.02 monolayer as $n \rightarrow \infty$. This value is considerably smaller than the maximum observed in our experiments (Fig. 17). However, based on the observed relative flux of hydrogen atoms surviving transit through the reactor with the gold specimen ($Q_H/Q_H^* = 0.62$), it is evident that a significant fraction of the incident atoms do not recombine. Consequently, k_3 was adjusted to a lower value (2×10^{-9} $(atoms/cm^3)^{-1}$ min^{-1}) to give an isotherm in reasonable agreement with the data (Fig. 20).

The relative values of the rate constants indicate that adsorption is the rate-limiting process in the recombination of hydrogen atoms on gold. This conclusion is further supported by the similarity in value of the recombination coefficient γ determined previously[2] at a relatively high pressure ($P_H \cong 10^{-3}$ torr; $\gamma = 0.072$) and the clean-surface sticking coefficient ($S = 0.065$). We may compute k_3 from this value of γ on the basis of first order Eley-Rideal kinetics[2]:

$$k_3 = \frac{\gamma \bar{c}}{4N\theta}$$

where $\bar{c}$ is the mean atomic velocity. If we assume the high pressure limit of $\theta = 0.06$, this computation gives $k_3 = 4 \times 10^{-9}$ $(atoms/cm^3)^{-1}$ min^{-1}, in reasonable agreement with the value derived from our low pressure rate measurements.

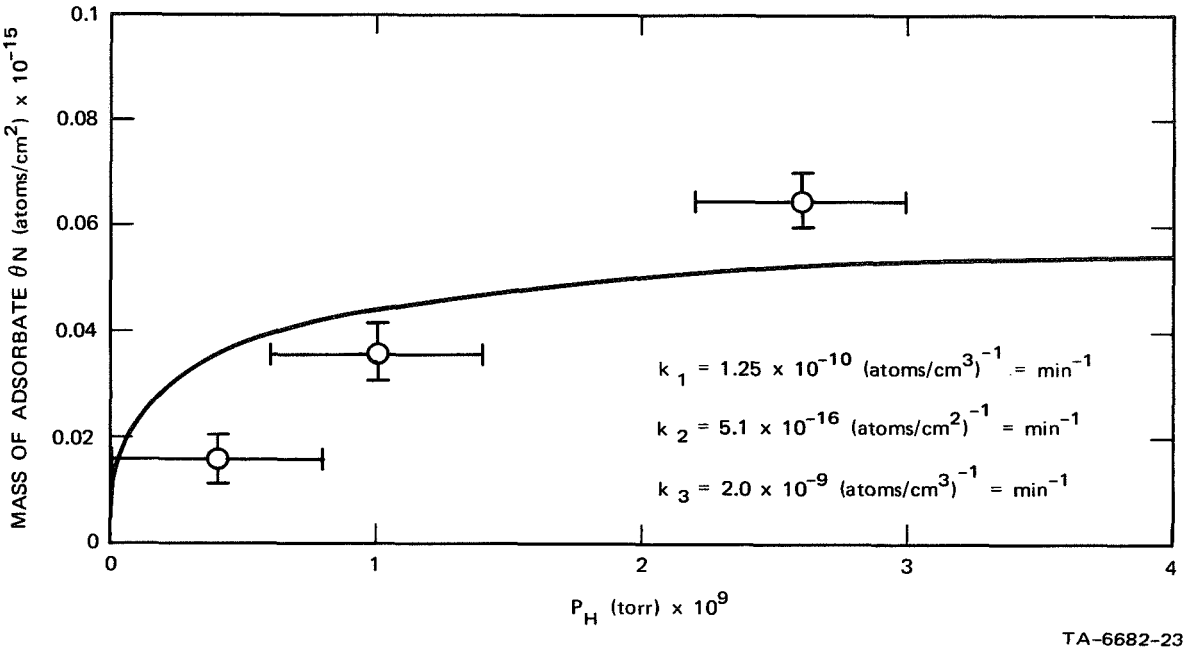

FIGURE 20 ISOTHERM FOR ATOMIC HYDROGEN ADSORPTION ON GOLD AT 300°K. Curve computed from Eq. 20 using indicated values for rate constants; experimental points from data in Figure 17.

2. Oxygen-covered Gold

The hydrogen atom concentration in the upper atmosphere is much smaller than that of oxygen atoms. This fact, considered together with the relatively high rate of adsorption of atomic oxygen on gold, suggests that one should be concerned with the rate and nature of the interaction between gaseous hydrogen atoms and oxygen adatoms.

We have investigated this reaction by means of the flash-filament technique. The gold ribbon specimen, flash cleaned, was exposed to a flux of atomic oxygen for a sufficient time to saturate the surface with a monolayer of adatoms. The oxygen supply to the system was then cut off, and, following a brief period of evacuation, hydrogen at a predetermined constant flux was admitted to the atom source and the reactor for a period of time. At the end of this exposure to hydrogen atoms, the hydrogen supply was interrupted and the ribbon was electrically heated to desorb residual adsorbed oxygen. We thus evaluated the mass of oxygen remaining on the gold surface after exposure to a constant flux of hydrogen atoms for various periods of time. The results, corrected for Langmuir-Hinshelwood oxygen atom recombination, are shown in Fig. 21. The initial rate, shown by the dashed line, is comparable to the incident flux of hydrogen atoms under the conditions of the experiment ($P_H \cong 5 \times 10^{-9}$ torr), and indicates that the reaction occurs with approximately unit efficiency. The products of the reaction could not be determined. A blank experiment, in which an oxygen-covered gold surface was exposed for 8 minutes to a flux of molecular hydrogen at $P_{H_2} \simeq 10^{-6}$ torr, indicated that the rate of reaction of gaseous molecular hydrogen with oxygen adatoms on gold is negligibly small.

C. Carbon Monoxide Adsorption

1. Gold

The sticking coefficient of CO on gold (Fig. 22) is nearly an order of magnitude less than that for atomic oxygen (Fig. 9). The saturation coverage observed in our experiments is about one-sixth that of oxygen, but it appears to exhibit a dependence on the CO pressure. A comparison of the room temperature desorption rate of oxygen and the sorption rate of CO, shown by the broken curve in Fig. 10, indicates

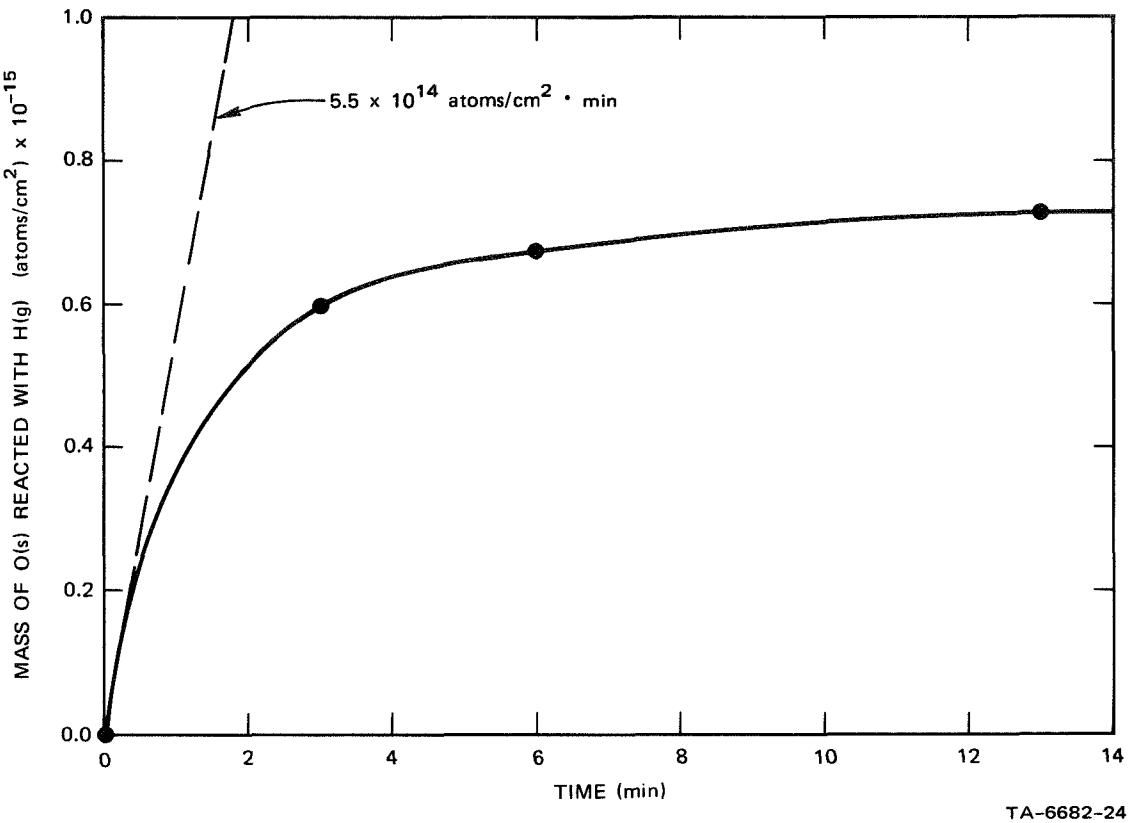

FIGURE 21 RATE OF REACTION OF GASEOUS ATOMIC HYDROGEN WITH OXYGEN ADATOMS ON GOLD AT 300°K. $P_H \cong 3 \times 10^{-9}$ torr. At time = 0, gold surface coverage with oxygen $\theta N = 1.07 \times 10^{15}$ atoms/cm^2.

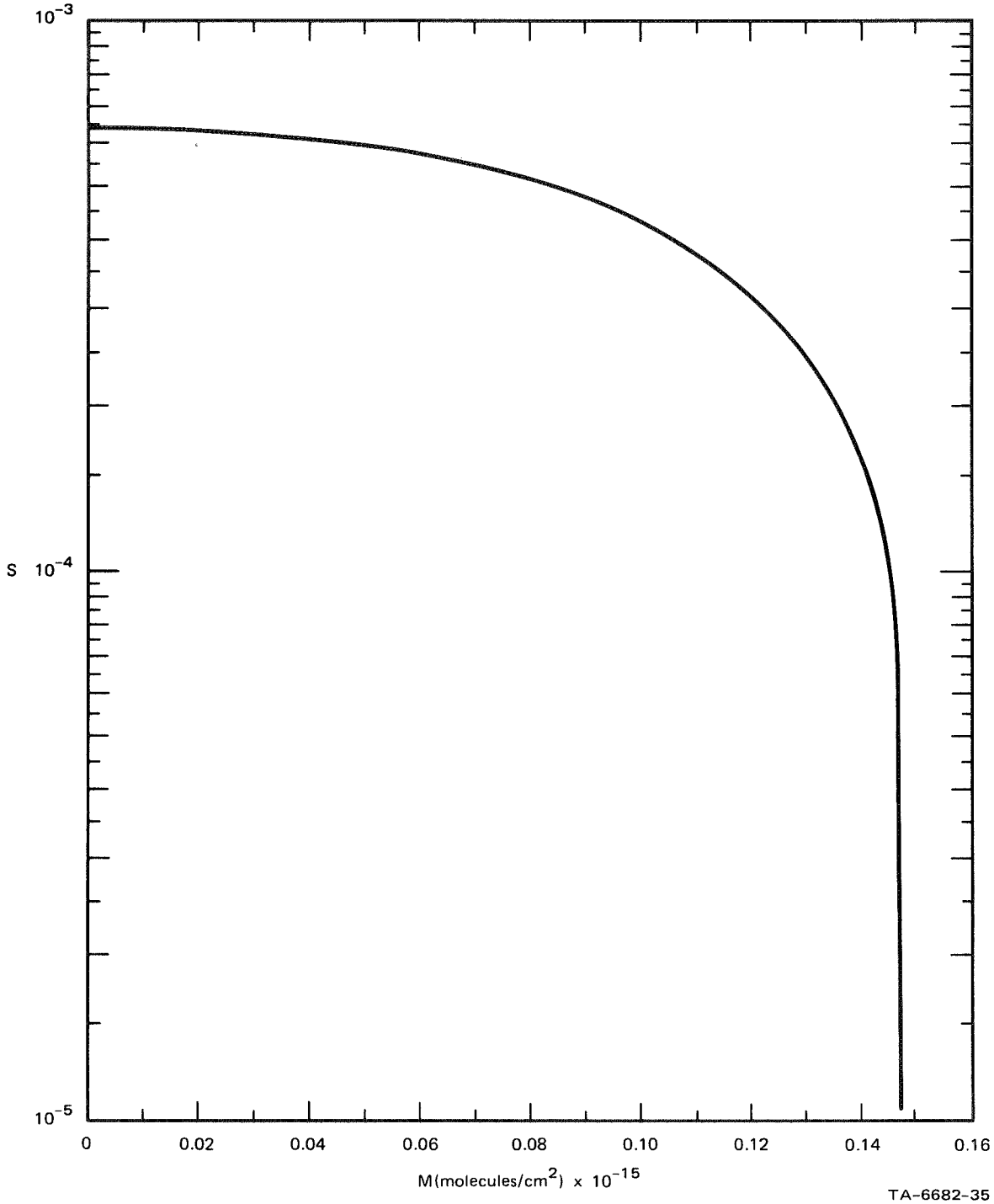

FIGURE 22 STICKING COEFFICIENT OF CO ON GOLD AT 300°K. $P_{CO} \cong 5 \times 10^{-6}$ torr.

that displacement of sorbed oxygen by CO is not involved in the oxygen desorption mechanism.

2. Silver

We determined that CO sorbs on silver rather slowly, exhibiting a sticking coefficient of 0.003 in CO partial pressures to 10^{-6} torr. We found no evidence that CO interferes with the uptake of oxygen by silver in an atmosphere containing atomic oxygen. Such behavior seems quite reasonable in view of the reported[12] results of other investigations of oxygen uptake by silver after pretreatment with CO.

V. PRACTICAL CONCLUSIONS

The parameters we have evaluated in our laboratory experiment can be of value in interpreting data obtained from the OGO-F and other flight mass spectrometers. We here enumerate conclusions related to the various metal surfaces that we studied.

A. Gold

1. The time required to saturate the gold surface of an antechamber by atomic oxygen can be computed from the sticking coefficient. The variation of sticking coefficient with coverage is small, so that for practical purposes one can consider it constant up to full surface coverage.

2. For data obtained in an atmospheric region in which the antechamber surface can be considered to be saturated with sorbed oxygen, the value of amu 16 reported by the instrument should be corrected for atom loss by recombination in the antechamber. In principle, our theoretical model will permit precise corrections to be made for flight instruments with cylindrical antechambers, such as the OGO-F. The steady, high ratio of mass 32/mass 16 being reported by the OGO-F mass spectrometer at perigee[21] indicates that atom removal by recombination is a most significant process in the flight instrument's antechamber. This observation is in conformity with the behavior of gold predicted by our experimental results.

3. If the satellite, because of the eccentricity of its orbit, spends periods of many minutes in regions of low oxygen atom density,

the effect of desaturation of the antechamber surfaces must be taken into account. The fraction of the surface populated with oxygen atoms will exhibit a dynamic dependence on the rates of sorption (sticking coefficient) and desorption. The variation might be quite complex, but, in principle, should be tractable if the sorption/desorption rates derived from our experiments are used. If a means could be provided to keep the antechamber walls at a high temperature, oxygen atom sorption and recombination would be negligibly small, and these corrections would be obviated.

4. The high efficiency of the reaction between gaseous hydrogen atoms and oxygen adatoms on gold observed in our experiments seems to be in conflict with reports of hydrogen atom number densities of the order of 10^8 cm^{-3} reported by the OGO-F satellite mass spectrometer at perigee.[2] Since no ion fragments that could be attributed to water or to molecular hydrogen appear in the upper atmosphere mass spectrum, hydrogen atoms must survive transit through the sampling antechamber either as gaseous atoms or in some other combined form. We may speculate on two possible sources of hydrogen atoms.

a. Hydrogen atoms might react with surface sorbed oxygen to form the metastable radical, OH. At 300°K this species possesses a 9.4 kcal endothermic heat of formation,[10] so its generation from its constituent atoms, even where one of them is in an adsorbed state, is thermodynamically quite favorable. Such radicals would undoubtedly dissociate after a few collisions with the wall. However, the products would be the constituent atoms, for the number density of adsorbed hydrogen is so low that an encounter with a hydrogen adatom to form water is highly unlikely. In contrast, the probability that the hydrogen atoms from collision-dissociated OH would react with another oxygen adatom is high, and we can conceive that a hydrogen atom could survive transit through the sampling antechamber by successive formation and dissociation of OH radicals. In the ion source of the mass spectrometer, the probability is high that nearly all the OH radicals ionized by electron impact would be fractured into H^+ and O^+ ions. Consequently, only mass peaks at amu 1 and amu 16 would be observed. It has been reported[21]

that in the OGO-F mass spectrometer data, the intensity of the mass 16 peak demonstrates a slight increase in conjunction with increases of the mass 1 peak. This result, of course, is consistent with the proposed atom transport mechanism.

b. The source of the observed hydrogen might be nonatmospheric. It has been demonstrated[22] that hydrogen diffuses readily through gold at temperatures as low as 373°K. Hence, hydrogen occluded in the gold plating on the mass spectrometer antechamber surface (or even hydrogen included in the stainless steel substrate) would diffuse to the free surface where, by reaction with an oxygen adatom, it would leave the surface as an OH radical.

By making a number of reasonable assumptions, we can estimate the concentration of hydrogen at the gold-plate/steel interface required to maintain a steady-state number density of H = 10^8 cm^{-3} in the antechamber. Our assumptions are:

i) the gold surface is the sole source of hydrogen;

ii) the rate of arrival of atoms by diffusion from the solid, Ddn_s/dx, is balanced by their departure through the antechamber inlet orifice with flux ϕ;

iii) the concentration n_s of H(s) at the gold surface approaches zero;

iv) the diffusive concentration gradient of atoms in the gold is linear;

v) the thickness x of the gold-plate layer is 0.002 in. (5×10^{-3} cm).

From the dimensions of the antechamber and its orifice:[21]

$$\phi = Ddn_s/dx \cong 10^{11} \text{ atoms/sec.cm}^2 \qquad (21)$$

The diffusion coefficient D for hydrogen in gold at 300°K, obtained by extrapolation of available data,[23] is 5×10^{-8} cm^2/sec. Applying conditions iii, iv, and v to Eq. (21) gives a statement of the approximate value of the hydrogen concentration n_s at the gold-steel interface:

$$n_s \cong \frac{10^{11} x}{D} \cong 1.2 \times 10^{17} \frac{\text{atoms}}{\text{cm}^3} = 1.9 \times 10^{-7} \frac{\text{mole}}{\text{cm}^3}$$

The molar density of gold at 300°K is $9.8 \times 10^{-2} \frac{\text{mole}}{\text{cm}^3}$. Hence, the computed value of n_s represents a fractional hydrogen content of $1.9 \times 10^{-7} / 9.8 \times 10^{-2}$ or ~2 ppm. The presence of an occluded hydrogen concentration of this magnitude is quite plausible. Therefore, the solid surface of the mass spectrometer antechamber cannot be discounted as the source of the observed hydrogen (amu 1) peak. A critical analysis of the variation of amu 1 with altitude, relative to concurrent variations in amu 16, may provide further insight into the source of atomic hydrogen.

B. Silver

The insight into the interaction of oxygen atoms with silver obtained from our laboratory experiments may be of value in interpreting the oxygen atom concentration data reported by the silver-plated mass spectrometer of the Explorer XXXII aeronomy satellite. The principal mode by which atomic oxygen is lost on silver under our experimental conditions appears to be occlusion in the bulk. The rate of this process, however, may be dependent on the pressure of gaseous atoms; hence, a continuous correction based on the variation of the ambient oxygen atom pressure may be required to assess the significance of this process on atom loss.

C. Titanium

The complex behavior of titanium in the presence of atomic and molecular oxygen prompts us to conclude that use of this metal in or near the sampling chamber of a flight mass spectrometer requires passivation of the metal surface by pretreatment with oxygen. But the conditions under which such a passivated surface will be stable are not clearly established and may be difficult to attain in the upper atmosphere. As a result, variation in activity with exposure time is to be expected.

D. Stainless Steel

Since the mode of oxygen atom removal on a stainless steel surface is likely to depend on the prior history of the metal, it would be hazardous to attempt to make a prediction about it. The nature of the

interaction is important, however, because the appearance of CO_2 may be the direct product of an oxygen atom-surface reaction, in which case the magnitude of the CO_2 signal would provide a basis for correcting the atomic oxygen signal for surface loss. Consequently, there is no substitute for an empirical measurement of the kinetics and products of oxygen atom-surface interaction on stainless steel specimens of composition and prior treatment identical to those employed for the fabrication of the antechamber of a flight mass spectrometer. Such procedures can be obviated, of course, by avoiding the use of exposed stainless steel surfaces in favor of metals, such as gold, which exhibit no chemical interaction with gaseous atomic oxygen.

E. Aluminum

The highly inert and stable character of aluminum oxide-clad aluminum toward oxygen atoms indicates that this material might be quite acceptable as a material of construction for flight mass spectrometers. One note of caution should be raised. There is some evidence, from earlier, high-pressure, experiments carried out in our laboratory, that the aluminum oxide surface coating on an aluminum wire can be slowly reduced by prolonged exposure to atomic hydrogen. The hydrogen atom density in the upper atmosphere is very low; yet, over long periods of time such a surface change might occur, with consequent, unpredictable effect on the rate and nature of oxygen atom interaction.

F. Analytical Model

The apparent applicability of the analytical model to interpretation of experimental data obtained in a short reactor ($L/R_o \cong 2$) suggests that solutions of the model for a long reactor geometry ($L/R_o \cong 12$) would be of great value in interpretation of data from the OGO-F mass spectrometer. The antechamber in this instrument possesses a length/diameter ratio, $L/R_o \cong 11$. Consequently, refinement of this computational problem is considered to be of great importance to derive maximum practical benefit from the surface kinetic data obtained in this study.

VI. PERSONNEL

Personnel who have contributed to this study include Bill R. Baker, Bjorn W. Bergsnov-Hansen, Noboru Endow, Leon E. Hiam, Jan W. Van Gastel, Henry Wise, and Bernard J. Wood.

VII. PUBLICATION

A paper entitled "Competitive Sorption Kinetics of Oxygen and Carbon Monoxide on Platinum" by Bernard J. Wood, Noboru Endow, and Henry Wise has been accepted for publication by the Journal of Catalysis. This paper describes results obtained during preliminary experiments in the early stages of this project. A preprint of this paper constitutes Appendix B.

REFERENCES

1. U. von Zahn, J. Geophys. Res. 72, 5933 (1967) (a critical review).

2. H. Wise and B. J. Wood, Advances in Atomic and Molecular Physics, Vol. 3, New York, Academic Press, 1967, 296ff.

3. R. Courant and D. Hilbert, Methods of Mathematical Physics, Vol. 1, Interscience, New York, 1953.

4. E. M. Sparrow, L. V. Albers, and E.R.G. Eckert, J. Heat Transfer, 84C, 73-81 (1962).

5. A. Guthrie and R. K. Wakerling, Vacuum Equipment and Techniques, New York, McGraw-Hill Book Co., 1949, 12ff.

6. P. O. Schissel and O. C. Trulson, J. Chem. Phys. 43, 737 (1965).

7. W. Steckelmacher, Vacuum 11, 561 (1966).

8. G. Ehrlich, Advances in Catalysis 14, 255 (1963).

9. B.M.W. Trapnell, Proc. Roy. Soc. (London), A218, 566 (1953).

10. C. E. Wicks and F. E. Block, U. S. Bureau of Mines Bulletin 605 (1963); JANAF Thermochemical Tables, Dow Chemical Co.

11. M. J. McBee and H. T. Yolken, "Silver Oxidation in Atomic Oxygen," National Bureau of Standards Report 9802, March 25, 1968.

12. A. W. Czanderna, J. Phys. Chem. 68, 2765 (1964).

13. P. Kofstad, J. Less-Common Metals 12, 449 (1967).

14. D. B. Roach, W. B. Leffingwell, and A. M. Hall in "Advances in the Technology of Stainless Steel and Related Alloys," ASTM Special Tech. Publ. No. 369, Philadelphia, Pa., 1965, pp. 1-7; H. E. McGannon, editor: The Making, Shaping, and Treating of Steel, Pittsburgh, U. S. Steel Corp., 1964, 1111ff.

15. W. T. Kasprzak, D. Krankowsky, and A. O. Nier, J. Geophys. Res. 73, 6765 (1968).

16. A. O. Nier, private communication; W. T. Kasprzak, "The Structure of the Lower Thermosphere," Ph.D. Thesis, University of Minnesota, Minneapolis, December 1968, pp. 96-134.

17. A. O. Nier, J. H. Hoffman, C. Y. Johnson, and J. C. Holmes, J. Geophys. Res. 69, 979 (1964); ibid., 4629.

18. H. Marsh, T. E. O'Hair, and W.F.K. Wynne-Jones, Trans. Faraday Soc. 61, 274 (1965).

19. P. Hartek, R. R. Reeves, Jr., K. Loomis, and A. S. Bergendahl, Technical Status Report No. 4, Rensselaer Polytechnic Institute, Troy, N. Y. NASA Research Grant No. NGR-33-018-086. April 30, 1969.

20. G. C. Moore and F. C. Unterwald, J. Chem. Phys. 40, 2639 (1964).

21. D. N. Harpold, private communication.

22. B. J. Wood and H. Wise, J. Catalysis 5, 135 (1966).

23. W. Eichenauer and D. Liebscher, Z. Naturforsch. 17a, 355 (1962).

24. P. Clausing, Ann. Physik 12, 961-989 (1932).

25. M. Abramowitz and A. A. Stegun, Handbook of Mathematical Functions, National Bureau of Standards, App. Math. Series 55, Washington, D. C., 1964.

26. Y. N. Lyubitov, Molecular Flow in Vessels, translated from Russian by Consultants Bureau, New York, 1967.

APPENDIX A

The integral for the influence function of Eq. (4) can be evaluated for certain elements such as bands of a cylindrical surface by special methods which have been developed by Clausing[24] and which are also described in Sparrow et al.[4] and Steckelmacher.[7] However, the case of two general conical ring elements shown in Fig. 3c can also be handled conveniently by vector algebra.

We use triples of numbers enclosed in parentheses to designate components of a vector or the position vector of a point with respect to the Cartesian system shown in Fig. 3. For example, points in the two shaded area elements are

$$A: \quad (a,o,o) \qquad B: \quad (b\cos\theta,\ b\sin\theta,\ z) \tag{22}$$

The unit normals at those points are

$$n_A: \quad (\sin\beta_A,\ 0,\ \cos\beta_A) \qquad n_B: \quad (\sin\beta_B\cos\theta,\ \sin\beta_B\sin\theta,\ \cos\beta_B) \tag{23}$$

The vector from A to B is

$$AB = (b\cos\theta - a,\ b\sin\theta,\ z) \tag{24}$$

with length ℓ given by

$$\ell^2 = |AB|^2 = a^2 + b^2 + z^2 - 2ab\cos\theta \tag{25}$$

The inner products of the unit normal vectors with AB give

$$|\ell\cos\theta_A| = |AB\cdot n_A| = |\sin\beta_A\,(b\cos\theta - a) + \cos\beta_A\, z| \tag{26}$$

$$|\ell\cos\theta_B| = |AB\cdot n_B| = |\sin\beta_B\,(b - a\cos\theta) + \cos\beta_B\, z|$$

Direct substitution of these results into Eq. (4) gives

$$w_{AB} = \frac{1}{2\pi}\left|\int_0^{2\pi} \frac{[\sin\beta_A(b\cos\theta - a) + \cos\beta_A z]\,[\sin\beta_B(b - a\cos\theta) + \cos\beta_B z]}{[z^2 + a^2 + b^2 - 2ab\cos\theta]^2}\, d\theta\right| \tag{27}$$

Now we consider the basic integral (5) which can be found in standard tables (for example, formula 4.3.133 of AMS handbook[25]). The denomina-

tor of the integral (5) is ℓ^2, so it can never vanish. Hence, G is an analytic function of the parameters a, b, and z, and it can be differentiated with respect to them. The study of derivatives such as

$$2a \frac{\partial G}{\partial (a^2)} = \frac{\partial G}{\partial a} = - \frac{1}{2\pi} \int_0^{2\pi} \frac{2(a-b \cos \theta)\, d\theta}{[z^2 + a^2 + b^2 - 2ab \cos \theta]^2} \tag{28}$$

shows that Eq. (27) can be reduced to the form of Eq. (4).

By considering only special conical elements with β, either 0 or $\pi/2$ such as the rings (R) of the ends of the chamber of Fig. 1 or the bands (B) of the cylindrical surface, we can reduce Eq. (4) to the following standard influence functions given by Clausing[24] and Lyubitov[26]

$$\begin{aligned} w_{RR} &= z^2 \frac{a^2 + b^2 + z^2}{[(a^2 + b^2 + z^2)^2 - 4a^2b^2]^{3/2}} \\ w_{BB} &= \frac{1}{4R^2} \left\{ 1 - |z| \frac{6R^2 + z^2}{[4R^2 + z^2]^{3/2}} \right\} \\ w_{RB} &= w_{BR} = |z| R \frac{R^2 + z^2 - r^2}{[(R^2 + r^2 + z^2)^2 - 4R^2r^2]^{3/2}} \end{aligned} \tag{29}$$

APPENDIX B

COMPETITIVE SORPTION KINETICS OF OXYGEN AND CARBON MONOXIDE ON PLATINUM*

Bernard J. Wood, Noboru Endow, and Henry Wise

Department of Surface Chemistry and Physics
Stanford Research Institute, Menlo Park, California 94025

Abstract

The sorption of oxygen on a polycrystalline platinum ribbon has been studied with the aid of a quadrupole mass analyzer in an ultrahigh vacuum system in the pressure range from 5 to 10 x 10^{-8} torr. An evaluation of the reaction coefficient and the total mass of oxygen sorbed indicated that oxygen competes with carbon monoxide, present as a background contaminant ($P \simeq x\ 10^{-9}$ torr), for the sorption sites on the flash-cleaned platinum surface. Subsequent desorption of oxygen is not observed when the platinum is flash heated to temperatures up to 1100°K; carbon monoxide and carbon dioxide are the predominant species leaving the platinum surface. The relative amount of each component depends on the length of exposure of the flash-cleaned platinum ribbon to the background gas and to oxygen. The experimental results suggest a high reaction coefficient of oxygen on a clean platinum surface at room temperature ($S \simeq 0.2$).

* This research was supported by the National Aeronautics and Space Administration under Contract NASr-49(30).

Introduction

In view of the importance of the interaction between oxygen and metals in such areas as upper atmosphere composition studies, heterogeneous catalysis and catalyst surface-area determination, we have examined the adsorption and desorption characteristics of molecular oxygen on a clean platinum surface in a pressure region where rates of sorption can be conveniently measured ($\sim 10^{-7}$). We have also evaluated the role of an ubiquitous contaminant gas, carbon monoxide, on the kinetics and path of the sorption/desorption process.

Recent investigators have studied the surface chemistry of oxygen on platinum in the form of evaporated films,[1] foils,[2-4] single crystals,[5] and supported catalysts.[6-8] In all cases, a nonactivated process of chemisorption has been observed. The degree of surface coverage with oxygen has been a problem of major concern, with a limiting ratio of Pt/O = 2 generally assumed.

Experimental Details

The apparatus used for the experimental measurements (Fig. 1) was a Pyrex vessel consisting of two main sections (A and B) separated by shutter 1 and evacuated by separate ion-getter pumps. Chamber A (5 liters in volume) contained a quadrupole mass analyzer* which served the purpose of monitoring the pressure and composition of the gas mixture brought into contact with the platinum specimen. Chamber B (0.8 liter in volume), which contained the specimen, could be isolated from its pump by shutter 2. Both shutters were composed of two ground-glass discs, each pierced off center by a 3.5 cm diameter circular hole. One disc was attached to a central shaft and could be rotated relative to the other. The shutters were opened or closed by bringing the holes in or out of coincidence. Shutters 1 and 2 were ganged on a common shaft and so oriented relative to one another that when shutter 1 was open, shutter 2 was closed, and vice versa. The shutters were operated under vacuum by means of a "rotary-motion-feed-through."† The specimen was a ribbon of 99.95% pure foil (<1 ppm Carbon) (0.005 inch thick) spotwelded at its ends to glass-shielded tungsten wire supports. The ribbon, which had a geometric surface area of 2.4 cm^2, could be heated by passage of an electric current. Oxygen was admitted into chamber A from a high-pressure reservoir (10 to 100 torr) through a servo-operated valve‡ and a fixed conductance F (Fig. 1). The outflow of reactant from chamber A was controlled by a valve (conductance f, Fig. 1) leading to the 50 liter sec^{-1} ion getter pump.

Pressure measurements were made with inverted Bayard-Alpert type ionization gauges** operated with low temperature thoria-on-iridium

---

* Manufactured by EAI, Palo Alto, California
† Ultek Corp., Palo Alto, California
‡ Granville-Phillips Automatic Pressure Controller
** General Electric Co., Schenectady, New York

filaments. The mass spectrometer was calibrated with oxygen against ion gauge 2 in the range of 5×10^{-9} to 1×10^{-6} torr. The readings were found to be linearly related at pressures greater than about 5×10^{-8} torr for emission currents of 0.1 and 1.0 mA.

The experimental ratios of the pressures indicated by gauges 1 and 2 (Fig. 1) corresponded to those calculated from mass flow considerations. These results demonstrated that the pumping characteristics of the two gauges were similar in the range employed.

The gas-handling system could be operated in two modes: (1) the constant-flow condition, by fixing the rate of flow of reactant into chamber A, and (2) the constant-pressure condition, by controlling the leak rate through the servo-operated valve with signals received either from the total pressure gauge (ion gauge 2, Fig. 1) or from the quadrupole mass spectrometer (Fig. 1). Both modes of operation were employed in our experimental measurements.

In a typical constant-pressure experiment, a steady state pressure of oxygen at 1×10^{-7} torr was established in chamber A, while at the same time, the platinum ribbon in chamber B was cleaned by flash heating at 1100°K for 30 sec. Attempts to heat to higher flashing temperatures caused the ribbons to pull apart. Similar failures occurred when thinner ribbons were employed in hope of reducing the thermal inertia of the specimen. With the mechanically satisfactory 0.005" ribbons, a time interval of 120 sec was required for cooling of the ribbon to room temperature in a background pressure of 5×10^{-9} torr. Subsequently, chambers A and B were connected by closing shutter 2 and opening shutter 1, while the pressures monitored by ion gauges 1 and 2 were continuously recorded. The rate of sorption of oxygen on the platinum specimen (and the walls of chamber B, see below) was reflected in the observed change in gas flow into the system through the inlet conductance F. The sorption rate, R, is given by

$$R = F(P_1 - P_1') \tag{1}$$

where P_1' denotes the oxygen pressure in gauge 1 prior to exposure of the specimen, and P_1 that at time t. In addition, the total mass, M, of gas adsorbed at any time was evaluated by intergration of the area of the curve of P_1 versus time

$$M = \int_0^t F(P_1 - P_1') \, dt \tag{2}$$

The sequence of operations for the sorption experiments under isobaric conditions is presented in Table 1.

A blank experiment was carried out to determine the extent of oxygen sorption by surfaces other than the platinum specimen, such as the walls of chamber B. After completion of step 7 (Table 1) of the sorption measurement, chamber B was isolated and evacuated to the background pressure (5×10^{-9} torr) without flash cleaning of the platinum specimen. Subsequently, chambers A and B were connected (steps 5 and 6, Table 1). The mass of gas sorbed under these conditions was attributed to wall pumping since the platinum ribbon was covered with oxygen from the preceding experiment.

In the constant-flow experiments, the sorption process was followed by monitoring the decrease in total pressure and partial pressure of O_2 as a function of time by means of ion gauge 2 and the mass analyzer set at amu 32. The downstream conductance f was evaluated in the conventional manner by calculating the mass flux from the steady state pressure readings at ion gauges 1 and 2. The wall pumping correction was made in a manner similar to that used in the isobaric experiments.

Desorption data were obtained both in the presence and absence of oxygen under constant-flow conditions. Desorption was accomplished by flashing the sample ribbon at the same temperature and at the same rate as in the initial cleaning procedure with shutter 1 open and with conductance F fixed (steps 6-10, Table 1).

Results

The kinetic results obtained in a typical experiment for the sorption of oxygen on "clean" platinum are shown in Fig. 2. These measurements refer to the constant-pressure mode of operation at two platinum temperatures and various lengths of heating time during flash cleaning. The sorption kinetics are expressed in terms of a reaction coefficient, S, which represents that fraction of the incident molecules which adsorb (or react) on the surface.[4,9]

$$S = R/ZA \tag{3}$$

where Z is the collision frequency and A the geometric area of the platinum specimen.

Since Z may be expressed in terms of the product of the impingement rate ν and the oxygen pressure (torr-liter sec^{-1}), one obtains by substitution from Eq. (1)

$$S = [F(P_1 - P_1')]/(A\nu P_2) \tag{4}$$

In the experiments just described, ion gauge 2, which reflects the total pressure in the system, controlled the mass flux into the system at any time during the constant-pressure sorption measurement. In other experiments, the signal of the mass analyzer set at amu 32 was employed to govern the influx of oxygen into the system as demanded by

the sorption process for constant-pressure operation. All other conditions including the cleaning procedure were maintained. At a steady state pressure of oxygen of 1×10^{-7} torr, the platinum surface at 298°K sorbed 1.7×10^{-6} torr-liter of O_2 which compares favorably with a value of 2.3×10^{-6} torr-liter observed with the ion gauge. The difference is undoubtedly due to the different response of the two instruments to CO present as a background contaminant.

Of considerable interest are the results obtained from a series of desorption measurements (Table 2). During these studies the total gas pressures (measured by ion gauge 2) and the partial pressures of several components (measured by the mass analyzer) were monitored as the platinum ribbon temperature was rapidly raised to 1110°K after completion of the sorption process at 298°K. No oxygen was desorbed from the surface when the ribbon heating was carried out in the presence of molecular oxygen ($P_{O_2} = 10^{-7}$ torr) at a steady state flow. As a matter of fact, the quadrupole mass analyzer showed that the partial pressure of oxygen diminished and the partial pressures of CO and CO_2 increased. In another experiment in which the ribbon was heated in a system evacuated to $<10^{-8}$ torr, similar results were obtained, i.e., no liberation of O_2 but desorption of CO and CO_2.

The relative distribution of CO and CO_2 appeared to depend on the time interval between flash cleaning of the platinum ribbon at a base pressure of 5×10^{-9} torr and exposure to a given gas pressure of O_2. It can be seen from the data presented in Table 2 that (1) the mass of O_2 sorbed decreases with dwell time of the platinum specimen in the background gas (at 5×10^{-9} torr), (2) the mass of CO_2 desorbed attains a maximum value, and (3) the mass of CO desorbed increases. The origin of the CO in the system is not known precisely, but the mass analyzer indicated that at the base pressure of 5×10^{-9} torr about 80% (by volume) of the residual gas is carbon monoxide. Based on this concentration, and on the mass of CO and CO_2 recovered from the platinum surface after various sorption time intervals (Table 2), we estimate that CO sorbs with an initial sticking efficiency approaching unity.

Discussion

Since the oxygen sorbed on the platinum specimen is not recovered as O_2, we conclude that chemical reaction occurs on the surface between the oxygen and the platinum and other sorbed species. Based on the observed residual partial pressure of CO in the vacuum system and on the identification of the desorbed gas as CO_2, we conclude that a primary chemical process occurring on the surface is the catalytic oxidation of CO to CO_2.

The disparity in the mass balance between sorbed and recovered gas (Table 2) can be accounted for by proposing a second chemical reaction at the surface to form a platinum oxide[10] (such as PtO or PtO_2). Platinum oxides are known to be volatile[11] under the conditions of temperature and oxygen pressure employed in our experiments. Hence, it seems likely that, upon heating, the fraction of the surface-sorbed oxygen which does not react with sorbed CO volatilizes as PtO or PtO_2. These species would be present at concentrations below the limits of detection of our apparatus and could condense on adjacent cool surfaces.

The diminution in mass of oxygen sorbed with increasing dwell time of the cleaned specimen in the evacuated system suggests that CO sorption pre-empts sites that would otherwise be available for oxygen. For reaction to occur, both O_2 and CO need to be chemisorbed. The data suggest that CO_2 is not chemisorbed at room temperature.

On the basis of these observations a mechanism may be postulated to describe the interaction of oxygen and CO with a platinum surface:

CO sorption	$CO(g)$	$\rightarrow CO(s)$
Flash desorption preceding O_2 sorption	$CO(s)$	$\rightarrow CO(g)$
O_2 sorption and reaction with CO	$O_2(g)$	$\rightarrow 2O(s)$
	$O(s) + CO(s)$	$\rightarrow CO_2(s)$
Flash desorption following O_2 sorption	$O(s) + Pt$	$\rightarrow PtO(g)$
	$CO_2(s)$	$\rightarrow CO_2(g)$

To obtain some measure of the energy of adsorption of CO on Pt, we carried out a series of experiments in which the maximum temperature attained by the platinum ribbon during flash cleaning was limited to 815°K rather than 1100°K. Under these conditions, no subsequent uptake of oxygen by the ribbon could be detected. Using the "rule of thumb" that desorption occurs at a significant rate[12] when the specimen temperature is greater than $20(Q_d)$, where Q_d is the heat of adsorption, one obtains a value of $41 < Q_d < 55$ kcal/mole.

The value for the reaction coefficient of oxygen on platinum at 298°K is of the same magnitude as that reported by Vanselow and Schmidt[3] on a platinum ribbon. However, S appears to be strongly affected by the length of time the platinum filament was heated to 1100°K during the flash desorption step (Fig. 2). Similarly, the total mass of gas sorbed is a function of the duration of flash cleaning of the platinum ribbon at a background pressure of 5×10^{-9} torr (Table 3). As a matter of fact, there appears to be a proportionality between the mass of oxygen sorbed, M, and the reaction coefficient, S, as evidenced by the constant value obtained for the ratio M/S (Table 3). On the basis of these results, we conclude that the duration of flash cleaning at 1100°K was insufficient to completely remove the gases sorbed on the surface of our platinum ribbon. Undoubtedly the strong binding of chemisorbed oxygen by platinum, for which process an energy of adsorption of 67 kcal/mole has been reported,[1] is reflected in this result. Also, the temperature gradients

in the platinum ribbon during flash heating add to the problem of completely removing the sorbed layer.

Several investigators[3,5] have reported that the upper limit of sorbed oxygen coverage corresponds to a ratio Pt/O = 2.* This degree of surface coverage would correspond to 6×10^{14} atoms/cm^2, assuming 1.2×10^{15} Pt atoms/cm^2 on the basis of a surface area of 8.1 Å^2/Pt atom, averaged over the various crystal orientations.[13] The highest surface density of adsorbed atoms attained in our experiments was 2×10^{14} atoms/cm^2. If the relationship between total mass sorbed and reaction coefficient were to be maintained up to a surface coverage of 6×10^{14} oxygen atoms/cm^2, one would expect an initial value of S = 0.2. Such reaction coefficients are comparable to those obtained for hydrogen on platinum.[14] Our experimental results confirm the nonactivated chemisorption of oxygen on platinum as is found to be the case with hydrogen.

As for the competitive and pre-emptive adsorption of carbon monoxide, the data obtained emphasize the problems associated with oxygen sorption on platinum as a method for surface-area determinations. Obviously the product of reaction coefficient and partial pressure of gas need to be considered in an evaluation of the relative importance of the sorption kinetics of the individual gaseous components. In a conventional vacuum system operating at moderate background pressures of 10^{-6} to 10^{-5} torr, of which a large proportion may be made up of carbon monoxide with a reaction coefficient approaching unity, one can expect up to 10^{15} sites occupied each second. Thus for a supported catalyst with platinum surface area of 1 m^2 complete coverage might be expected within about 100 minutes of exposure to the background. It must be concluded therefore that prolonged exposure of a platinum catalyst of moderate surface area to the background gas of a vacuum system operating at 10^{-6} torr may lead to high carbon monoxide coverage that will falsify the surface area determination on subsequent sorption of oxygen.

* In a recent paper (Surface Sci. 12, 405 (1968), Morgan and Somorjai report that oxygen does not sorb at all on the (100) surface of a platinum single crystal. These authors suggest that prior contamination or a different crystal face may be prerequisite to oxygen chemisorption.

Acknowledgment

We gratefully acknowledge the contribution of Mr. Jan W. Van Gastel to the design and fabrication of the experimental apparatus.

References

1. D. Brennan, D. O. Hayward and R. Trapnell, Proc. Roy. Soc. A256, 81 (1960).
2. O. V. Krylov and S. Z. Roginskii, Dokl. Akad. Nauk SSSR 88, 293 (1953).
3. R. Vanselow and W. A. Schmidt, Z. Naturforsch. 21A, 1690 (1966); 22A, 717 (1967).
4. R. Gibson, B. Bergsnov-Hansen, N. Endow, and R. A. Pasternak, Trans. 10th Nat. Vacuum Symp. 88 (1964).
5. C. W. Tucker, J. Appl. Phys. 35, 1897 (1964).
6. H. L. Gruber, J. Phys. Chem. 66, 48 (1962).
7. V. S. Boronin, V. S. Nikulina, and O. M. Poltorak, Russian J. Phys. Chem. 41, 1443 (1967).
8. J. E. Benson and M. Boudart, J. Catal. 4, 704 (1965).
9. R. A. Pasternak, N. Endow, and B. Bergsnov-Hansen, J. Phys. Chem. 70, 1304 (1966).
10. J. H. Norman, H. G. Staley, and W. E. Bell, J. Phys. Chem. 71, 3686 (1967).
11. G. C. Freiburg and H. M. Petrus, J. Electrochem. Soc. 108, 496 (1961).
12. P. A. Redhead, J. Hobson, and E. V. Kornelsen, in Advances in Electronics and Electron Physics, L. Marton, Ed., Academic Press, New York, 1962.
13. H. Chon, R. A. Fisher, and J. G. Aston, J. Amer. Chem. Soc. 82, 1055 (1960).
14. D. Brennan and P. C. Fletcher, Trans. Faraday Soc. 50, 1662 (1960).

Table 1

EXPERIMENTAL PROCEDURE

Operation	Inlet Valve	P_2[a] (torr)	P_3[a] (torr)	Shutter 1	Shutter 2	Specimen Temp. (°K)
(1) Starting condition	Closed	$<5 \times 10^{-9}$	$<5 \times 10^{-9}$	Closed	Open	298
(2) Inlet valve control set to admit O_2 and stabilize P_2	Open	1×10^{-7}	$<5 \times 10^{-9}$	Closed	Open	298
(3) Specimen heated (cleaned)	Open	1×10^{-7}	Peaks	Closed	Open	1113
(4) Specimen cooled	Open	1×10^{-7}	$<5 \times 10^{-9}$	Closed	Open	298
(5) Sorption commenced. Rate of sorption and quantity sorbed measured by recording P_1	Open	1×10^{-7}	1×10^{-7}	Open	Closed	298
(6) Sorption completed	Open	1×10^{-7}	1×10^{-7}	Open	Closed	298
(7) System evacuated	Closed	1×10^{-8}	1×10^{-8}	Open	Closed	298
(8) Specimen heated (desorbed); total quantity of all gas desorbed evaluated from ΔP_2; identity of gas established with quadrupole analyzer	Closed	Peaks	Peaks	Open	Closed	1113
(9) Specimen cooled	Closed	1×10^{-8}	1×10^{-8}	Open	Closed	298
(10) Starting condition restored	Closed	$<5 \times 10^{-9}$	$<5 \times 10^{-9}$	Closed	Open	298

a Subscripts refer to ion gauges identified in Fig. 1.

Table 2

EFFECT OF BACKGROUND GAS ON OXYGEN SORPTION BY PLATINUM AT 298°K
(Base pressure = 5×10^{-9} torr, oxygen pressure = 1×10^{-7} torr)

Dwell Time after Flash Cleaning (sec)	Mass of O_2 Sorbed (torr-liter $\times 10^6$)	Mass Desorbed[a]/ (torr-liter) $\times 10^6$		
		amu 28	amu 32	amu 44
120	2.3	0.2	0	1.5
240	1.9	--	0	4.5
600	1.6	--	0	2.9
3,000	0.6	16	0	--
300,000	0	20	0	--

[a] Quadrupole mass analyzer calibrated using O_2 with ion gauge.

Table 3

EFFECT OF FLASH-CLEANING TIME ON OXYGEN SORPTION BY PLATINUM RIBBON AT 298°K[a]

Flash-Cleaning Time at 1100°K (sec)	Mass O_2 Sorbed at Saturation, M (atoms/cm^2 $\times 10^{-13}$)	Pt/O[b]	Reaction Coefficient S	M/S $\times 10^{-15}$
30	6.5	18	0.023	2.8
155	15.0	8	0.063	2.4
180	18.4	6	0.075	2.5

[a] The platinum ribbon was allowed to cool for 120 sec before exposure to oxygen at $P = 5 \times 10^{-8}$ torr.

[b] Based on 1.2×10^{15} surface atoms of Pt per square centimeter of area.

Figure Captions

Fig. 1 Schematic diagram of experimental apparatus

Fig. 2 Reaction coefficient of oxygen on platinum as a function of surface coverage and temperature. Time values indicate duration of heating during presorption cleaning.

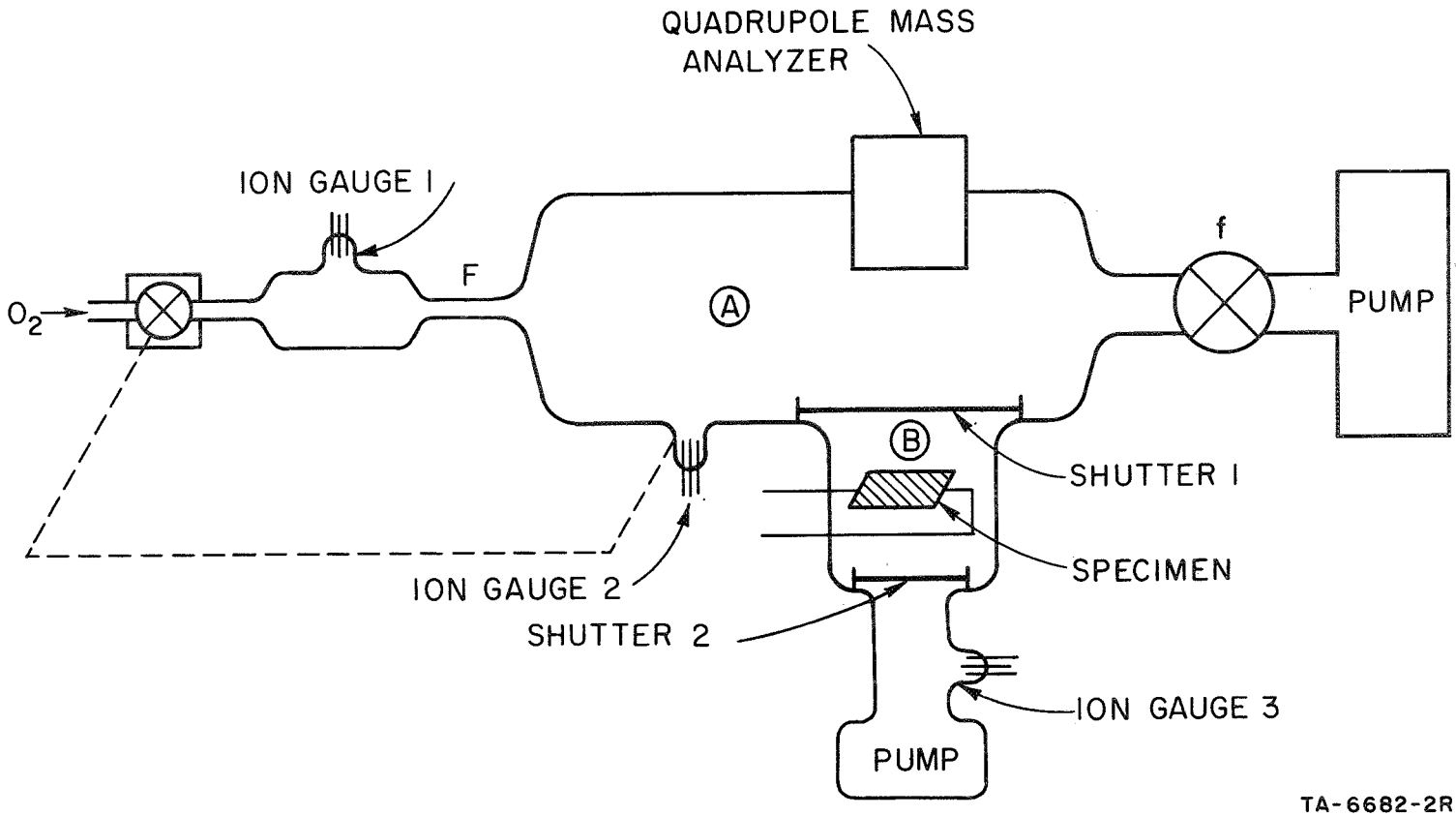
QUADRUPOLE MASS
ANALYZER
ION GAUGE 1
F
f
O_2
A
PUMP
B
SHUTTER 1
SPECIMEN
ION GAUGE 2
SHUTTER 2
ION GAUGE 3
PUMP
TA-6682-2R

FIG. 1

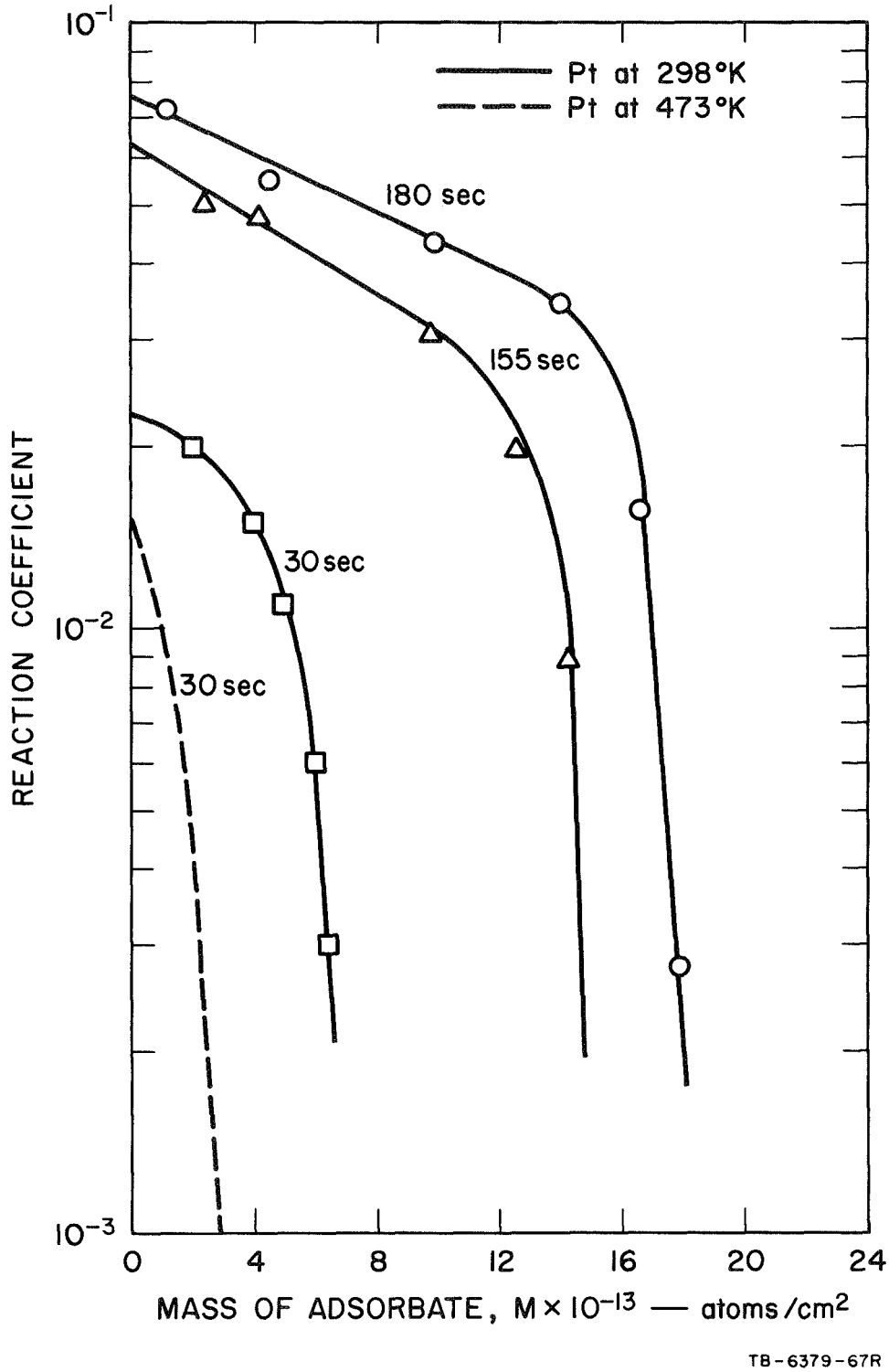
Pt at 298°K
Pt at 473°K
180 sec
155 sec
30 sec
30 sec
REACTION COEFFICIENT
10^{-1}
10^{-2}
10^{-3}
0
4
8
12
16
20
24
MASS OF ADSORBATE, M × 10^{-13} — atoms/cm^2
TB-6379-67R

FIG. 2